Atmospheric Environment 377 (2026) 122044

Contents lists available at ScienceDirect

Atmospheric Environment

journal homepage: www.elsevier.com/locate/atmosenv

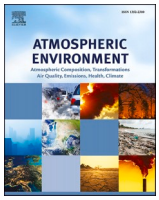

Source apportionment of particulate matter and its oxidative potential in an urban-industrial hot spot of Central Italy

Lorenzo Massimi [a,*,1], Alice Zara [a,1], Caterina Tiraboschi [a,b], Mara Galletti [c], Marco Vecchiocattivi [c], Silvia Canepari [a]

[a] Department of Environmental Biology, Sapienza University of Rome, Rome, 00185, Italy
[b] Department of Public Health and Infectious Diseases, Sapienza University of Rome, Rome, 00185, Italy
[c] ARPA Umbria, Regional Environmental Protection Agency, Terni, 05100, Italy

HIGHLIGHTS

- One-year source apportionment of PM_{10} by PMF and of OP^{DTT}, OP^{AA}, and OP^{DCFH} by MLR.
- PM_{10} dominated by biomass burning (29%), traffic (20%), and soil dust (17%).
- OP^{DTT} strongly correlated with urban sources (biomass burning 36% and traffic 24%).
- OP^{AA} driven mostly by traffic (44%), OP^{DCFH} by biomass burning (42%).
- Multiple OP assays are useful due to the distinct specificities of emission sources.

ARTICLE INFO

Keywords:
PM_{10}
OP^{DTT}
OP^{AA}
OP^{DCFH}
PMF
MLR

ABSTRACT

One-year PM_{10} monitoring was conducted in a hot spot of Central Italy in 2022. The study area is an open-air laboratory for in-depth investigation into PM emissions and their health effects due to the presence of intense residential and industrial sources. PM_{10} was collected daily on quartz filters using a high-volume sampling system to obtain a comprehensive chemical characterization, including OC, EC, levoglucosan, ions, macro-, micro-, and trace elements, as well as the measurement of OP of PM_{10} by employing OP^{DTT}, OP^{AA}, and OP^{DCFH} assays. Source apportionment of PM_{10} mass concentration and its OP was performed by PMF and MLR, respectively. PMF analysis identified 7 main emission sources of PM_{10}: biomass burning for home heating, vehicular traffic including exhaust and non-exhaust emissions, two steel plant sources, soil dust, sea spray, and secondary inorganics. PM_{10} mass concentration was dominated by biomass burning (29%), vehicular traffic (20%), and soil dust (17%). Source apportionment of OP by MLR revealed a differential sensitivity among the three OP assays: OP^{DTT} responded significantly ($p < 0.05$) to urban sources (biomass burning 36%, vehicular traffic 24%), steel plant emissions (10%), and secondary inorganic species (18%), OP^{AA} to vehicular traffic (43%), and OP^{DCFH} to biomass burning (42%). These distinct specificities underscore why the employment of multiple assays is useful for the assessment of OP of PM_{10} and highlight the need for further research to elucidate the accuracy of OP assays in reflecting oxidative stress mechanisms and health effects, calling for caution in adopting OP as a regulatory metric.

1. Introduction

Atmospheric particulate matter (PM) poses a significant threat to human health, with exposure linked to a range of acute and chronic diseases (Schraufnagel et al., 2019a; Schraufnagel et al., 2019b; Al-Kindi et al., 2020; Kyung and Jeong, 2020), including endocrine disruption, heart disease, stroke, chronic obstructive pulmonary disease (COPD), and lung cancer (Novák et al., 2020; Rychlik et al., 2019; Plunk and Richards, 2020; Arias-Pérez et al., 2020; Bălă et al., 2021; WHO, 2021; Kaur et al., 2022). The health impact of PM is usually evaluated using

* Corresponding author.
E-mail address: l.massimi@uniroma1.it (L. Massimi).
[1] These authors have contributed equally to this work and share first authorship.

https://doi.org/10.1016/j.atmosenv.2026.122044
Received 25 December 2025; Received in revised form 25 March 2026; Accepted 29 April 2026
Available online 30 April 2026

mass concentration as the key exposure metric (Pétremand et al., 2022; Sanda et al., 2023), a practice supported by the European Air Quality Directives 2008/50/EC and 2024/2881/UE, which established, respectively, annual mean limit and target values for $PM_{2.5}$ and PM_{10} mass concentrations. However, since PM is a heterogeneous mixture of components with very different chemical-physical properties originating from various emission sources (Bi et al., 2019; Adam et al., 202; He and Zhang, 2023), understanding the chemical profiles and contributions of these different sources to the overall PM mass concentration is essential. This knowledge is crucial for developing effective control and mitigation strategies (Zhao et al., 2020), enabling informed decision-making for pollution management (Li et al., 2020), and ultimately improving air quality and public well-being (Barrington-Leigh et al., 2019; Corvalan et al., 2005). To this aim, various statistical techniques are usually used for PM source apportionment, such as the Positive Matrix Factorization (PMF), a widely employed receptor model for quantifying source contributions to PM (Jeong et al., 2017; Jain et al., 2017; Ashrafi et al., 2018; Xu et al., 2021; Ali-Taleshi et al., 2022). Nevertheless, PMF-based source apportionment demands extensive datasets, requiring the collection of a large number of PM samples and the analysis of numerous chemical components, making it time-consuming and costly (Xu et al., 2023). Consequently, the source-specific mass contribution to PM remains unassessed in some highly polluted urban-industrial contexts. Furthermore, industrial settings may have emission sources that, despite a limited contribution to overall PM mass, release chemical compounds with the potential to induce adverse health effects even at relatively low exposure levels (Ali et al., 2019; Massimi et al., 2020b, 2022). This underscores the importance of evaluating exposure metrics beyond PM mass concentration that can better reflect the toxicological potential of PM from different sources.

The harmful effects of PM, including inflammation, genotoxicity, and cell death, are primarily mediated by mechanisms of oxidative stress (Arias-Pérez et al., 2020; Santibáñez-Andrade et al., 2023). Oxidative stress represents an imbalance between oxidizing and antioxidant species at the cellular level (He and Zhang, 2023), initiating a cascade of inflammatory processes that increase susceptibility to cardiovascular and pulmonary diseases (Daellenbach et al., 2020). In recent years, novel methodologies have emerged to evaluate the health impacts of PM (Vaccarella et al., 2025a), with OP increasingly used as a proxy for the ability of particles to generate reactive oxygen species (ROS) and induce oxidative stress (Bates et al., 2019). However, the relationship between acellular OP and actual biological effects remains an area of ongoing investigation, and further studies are needed to clarify its correlation with cellular toxicity (Ayres et al., 2008; Costabile et al., 2023; Crobeddu et al., 2017; Di Iulio et al., 2025). Several studies conducted in Italy and across Europe have explored these aspects, highlighting both the potential and the limitations of OP as a health-relevant metric (Abrams et al., 2017; Øvrevik, 2019; Lionetto et al., 2021; Melzi et al., 2024; Vernocchi et al., 2025). Despite these uncertainties, OP represents a promising exposure metric to investigate the potential health effects of PM from different sources, taking into account the complexity of particle chemical composition. Several OP assays have been developed and applied (Molina et al., 2020). The dithiothreitol (OP^{DTT}) and ascorbic acid (OP^{AA}) assays quantify the consumption of these antioxidants by PM over time, reflecting the intrinsic capacity of particles to deplete antioxidants and consequently generate ROS. Conversely, the 2′, 7′−dichlorofluorescein (OP^{DCFH}) assay quantifies particle-bound ROS by measuring the fluorescence rate of DCFH, a non-fluorescent reagent that is oxidized to fluorescent dichlorofluorescein (DCF) upon reaction with ROS in the presence of horseradish peroxidase (Massimi et al., 2024).

Notably, in the new Air Quality Directive 2024/2881/EU (Linares et al., 2025), OP has been proposed as a parameter to be measured alongside PM mass concentration to better assess its health impact (Beloconi and Vounatsou, 2023). However, despite the ability of OP assays to account for the different chemical-physical properties of PM, some critical issues remain. Although correlations between OP and oxidative stress biomarkers have been identified (Costabile et al., 2023; Di Iulio et al., 2025; Melzi et al., 2024), the biological representativeness of each OP assay remains unclear (Vaccarella et al., 2025a). These assays exhibit different sensitivity to various PM components (Frezzini et al., 2022; Massimi et al., 2020a), and due to synergistic or competitive interactions among different redox-active species in PM (Ngoc Thuy et al., 2024; Pietrogrande et al., 2022), the sources that predominantly contribute to OP are not yet fully understood and vary across different assays and studies (Vaccarella et al., 2025a). While over the last few years several studies have attempted to apportion OP by linear regression-based models such as PMF and Multi-Linear Regression (MLR) (Cesari et al., 2019; Daellenbach et al., 2020; Weber et al., 2021; Dominutti et al., 2023; In 't Veld et al., 2023; Serafeim et al., 2023), inconsistent results have been reported across different geographical areas, identifying different emission sources as primary contributors to the various OP metrics. For instance, OP^{DTT} is frequently associated with combustion-related sources, including biomass burning and vehicular emissions, due to its sensitivity to both redox-active organic compounds and transition metals (Daellenbach et al., 2020; Serafeim et al., 2023; Weber et al., 2021). In contrast, OP^{AA} is commonly linked to non-exhaust traffic emissions, particularly brake wear, reflecting its strong dependence on transition metals such as Cu and Fe (Cesari et al., 2019; Dominutti et al., 2023; Massimi et al., 2020a, 2024). Conversely, OP^{DCFH} has been reported to be more sensitive to combustion-derived particles and secondary oxidative processes, often showing stronger associations with biomass burning, vehicular traffic, and atmospheric aging (Daellenbach et al., 2020; Massimi et al., 2025; Vaccarella et al., 2025a; Vernocchi et al., 2025). However, several studies have also identified different dominant sources depending on site-specific emission profiles, atmospheric conditions, and PM chemical composition, with contributions alternatively attributed to traffic, biomass burning, industrial emissions, and secondary aerosols. This variability highlights the complexity of OP responses and indicates that the relationship between emission sources and OP is not universal but strongly context-dependent.

Quantifying the contribution of individual PM sources to OP in urban and industrial contexts is crucial, as this information can, on the one hand, improve our understanding of the PM components and sources contributing to OP, and on the other hand, facilitate the development of effective health-oriented air quality strategies and regulations (Stevanović et al., 2023). In this study, we performed source apportionment of PM_{10} and its OP^{DTT}, OP^{AA}, and OP^{DCFH} by using PMF and MLR, respectively, in the Terni basin, an urban-industrial hot spot of Central Italy characterized by the presence of several anthropogenic emission sources that can contribute differently to both the mass concentration and the OP of PM_{10} (Massimi et al., 2020a, 2022). Notably, the steel plant and its surrounding area within the basin constitute a 655-ha "Site of National Importance" (SIN of Terni-Papigno; Decree of the Ministry of the Environment of 08.07.2002, Official Gazette No. 234 of 05.10.2002). While previous studies in this area have highlighted an increase in population mortality, hospitalizations, cancer incidence, and congenital malformations (SENTIERI, 2016; 2019, 2023), to the best of our knowledge, no prior research has focused on the source apportionment of PM and its OP in this context.

2. Materials and methods

2.1. Study area, sampling site, and equipment

Terni is a medium-sized city with a population of 112′000, situated in a 325 km^2 basin (Capelli et al., 2011) in the southwestern area of the Umbria region, Central Italy (42° 34′ N, 12° 39′ E; Fig. 1). Over the past decades, Terni underwent significant industrialization, becoming an important center for the steel and chemical industries (Adorno and Neri Serneri, 2009). Currently, the main industrial hub is the "Acciai Speciali

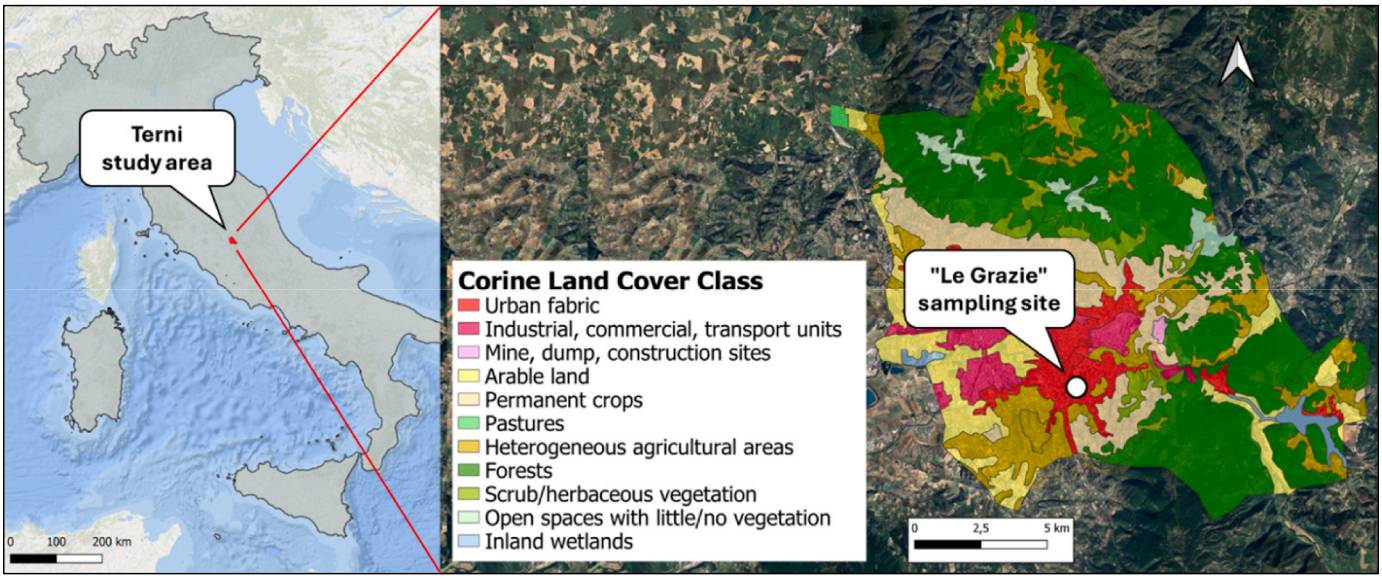

Fig. 1. Map of the sampling site in the study area (Terni, Central Italy) and land use and cover by CORINE Lanz et al., 2008; CLC 2018). Latitude: 42° 32′ 59.55″ N, Longitude: 12° 25′ 10.30″ E. (QGIS Development Team, 2022. QGIS Geographic Information System).

Terni" (AST) iron and steel plant. Additionally, typical urban PM emission sources exist within the city of Terni, such as biomass burning for domestic heating and vehicular traffic (Massimi et al., 2020b, 2022). The presence of several urban and industrial emission sources within the Terni basin, coupled with the peculiar geomorphological conditions of the basin that enhance atmospheric stability, promotes the accumulation of air pollutants often leading to the exceeding of the European daily limit values of PM_{10} mass concentration (50 μg m^{-3} with a limit of exceedance of 35 days per year; Air Quality Directive, 2008/50/EC, implemented in Italy by Legislative Decree No. 155 of August 13, 2010; UNION, 2008). Detailed information on meteorological conditions and atmospheric dynamics in the Terni basin has been previously reported (Ferrero et al., 2012; Guerrini, 2012; Moroni et al., 2013; Tositti et al., 2020) and is here considered representative of the study area.

PM_{10} sampling was carried out at the urban monitoring station "Le Grazie" (Fig. 1) of the Environmental Protection Agency of Umbria Region (ARPA Umbria) from January 14, 2022, to December 31, 2022. Although "Le Grazie" station is located within a municipal park, it is classified as a traffic and industrial site due to its proximity to busy roads and industrial areas (Fig. 1), such as the steel plant of the SIN, which makes it suitable for monitoring both urban and industrial PM emissions.

A high-volume sampling system (High Volume Aerosol Sampler DHA-80 DIGITEL) equipped with a PM_{10} sampling head was used to collect daily (24-h resolution, from midnight to midnight) PM_{10} all year round on 150 mm diameter quartz membrane filters (Whatman QMA). A

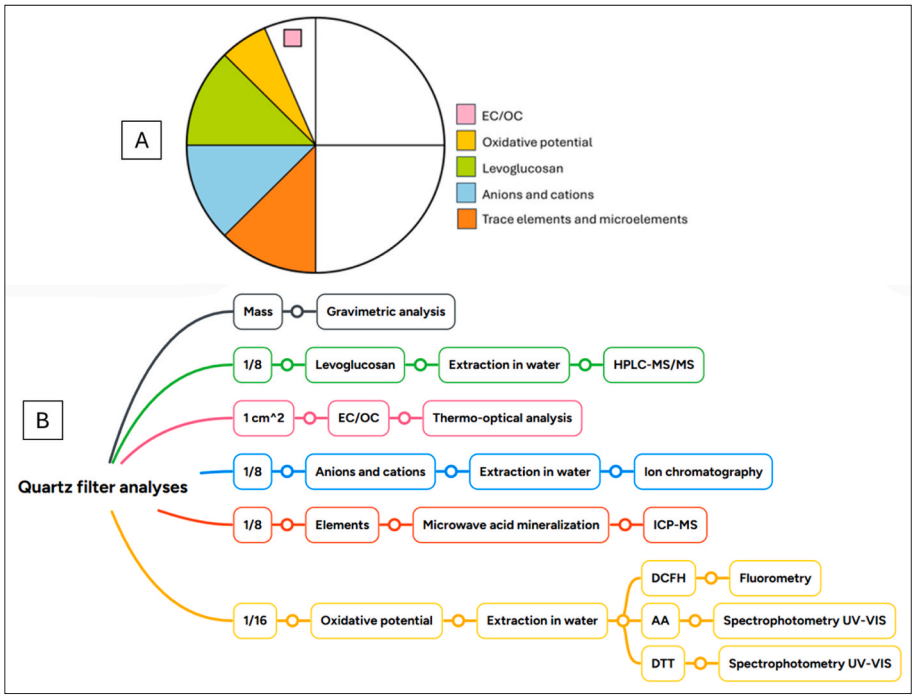

Fig. 2. Filter portions used for the analyses (panel A) and block diagram of the analytical procedure to which each portion was subjected (panel B).

total of 120 24-h PM_{10} quartz filters were selected for both chemical characterization and OP analysis using a homogeneous random sampling approach (approximately every three days).

2.2. Analytical procedure

To avoid replicate samplings and reduce costs, the number of analyses per sample was maximized, and a single quartz filter was used for multiple chemical analyses and OP^{DTT}, OP^{AA}, and OP^{DCFH} assays (Fig. 2). Only half of each filter was used, reserving the remaining portion for potential replicate analyses. To measure PM_{10} mass, each entire filter was weighed before and after sampling by using an automated microbalance (1 mg sensitivity, mod. ME5, Sartorius AG, Goettingen, Germany) after conditioning for 2 days at 20 °C and 50 % RH. Subsequently, as shown in Fig. 2, each filter half was divided into different portions for the following analyses: a 1 cm^2 punch was used for the determination of elemental carbon (EC) and organic carbon (OC); three eighths were allocated for the determination, respectively, of levoglucosan (LVGSN), anions and cations, micro- and trace elements; one-sixteenth was used for the measurement of OP^{DTT}, OP^{AA}, and OP^{DCFH}.

OC and EC were analyzed by thermo-optical analysis (CEN/TR 16243:2011, EUSAAR2 protocol) (Perrino et al., 2025). LVGSN was determined following the procedure detailed in Buiarelli et al. (2018). For anion and cation analysis, the filter portion was extracted with 10 mL of Milli-Q water in an ultrasonic bath for 60 min at room temperature (20–22 °C). The filtered (NC; 0.2 μm pore size; Merck Millipore Ltd., USA) extract was then analyzed using a DIONEX ICS-2100 IC for anions and an 881 COMPACT IC PRO METROHM for cations, according to MANUAL APAT IRSA CNR 29/200, Methods 4020 and 3030, respectively. Elemental analysis was performed according to UNI EN 14902:2005. This involved mineralizing the filter portion with 6 mL of HNO_3 (Honeywell Fluka, 69% trace select) and 2 mL of H_2O_2 (Supelco for ultratrace analysis, 30%) using microwave-assisted acid digestion (Ultrawave Milestone with quartz reactors). The resulting extract was diluted to 25 mL with Mill-Q water, filtered (NC; 0.2 μm pore size; Merck Millipore Ltd., USA), and analyzed by inductively coupled mass spectrometry (ICP-MS; Thermo Scientific, iCAP-RQ) using the internal standard calibration method (UNI EN 14902:2005). The analytical procedure applied in the present study is based on well-established methodologies previously optimized and validated, with minor adaptations to meet the specific objectives of this work. Further details on the chemical characterization procedures, calibration strategies, and analytical quality control for PM samples can be found in Canepari et al. (2006, 2009) and Massimi et al. (2022a).

Finally, for the OP assays, the filter portion was extracted in 10 mL of Milli-Q water by rotary agitation (60 rpm; Rotator; Glas-Col, USA) for 1 h. The resulting solution was then filtered through a nitrocellulose filter (NC; 0.45 μm pore size; Merck Millipore Ltd., USA). The water-extracted solution was subsequently divided into appropriate aliquots for the application of the OP^{DTT}, OP^{AA}, and OP^{DCFH} assays.

The OP^{DTT} assay was implemented as described by Fang et al. (2016) to determine the rate of DTT consumption. Three 0.7 mL aliquots of the water-extracted PM solution were prepared with 0.2 mL of 1 M phosphate buffer and 0.1 mL of 1 mM DTT and subsequently incubated at 37 °C. To measure the depletion, a 1 mL volume of 10% trichloroacetic acid (TCA) was added to one aliquot at regular intervals (0, 10, and 20 min) to stop the reaction. A reagent blank, consisting of all reagents processed under identical experimental conditions but without PM extract, was analyzed in parallel to account for background DTT consumption. The remaining DTT was then quantified by mixing 1 mL of the stopped solution with 2 mL of Tris-buffer (0.08 M, containing 4 mM EDTA) and 50 μL of 0.2 mM 5,5′-dithiobis-2-nitrobenzoic acid (DTNB). After 5 min, the absorbance was measured at 412 nm via UV-Vis spectrophotometry (Varian Cary 50). Finally, OPv^{DTT} or OPm^{DTT} was calculated as the DTT consumption rate per volume (nmol DTT $min^{-1}m^{-3}$) or mass (nmol DTT $min^{-1}\mu g^{-1}$) unit (Fang et al., 2016; Frezzini et al., 2022; Massimi et al., 2020a).

The OP^{AA} procedure was performed according to the methods established by Fang et al. (2016). To begin the reaction, 2.5 mL of the water-extracted solution from the PM sample was combined with 0.3 mL of 0.5 mM phosphate buffer and 0.1 mL of 2 mM ascorbic acid and kept in a thermostatic bath at 37 °C. The subsequent depletion rate of the AA was monitored by measuring the solution absorbance using UV-Vis absorption spectrometry (Varian Cary 50) at a 265 nm wavelength over three time points: 0, 10, and 20 min. A reagent blank, prepared and processed under the same conditions, was also used to correct for background AA depletion. The OPv^{AA} or OPm^{AA} value was then calculated as the AA depletion rate per volume (nmol AA $min^{-1}m^{-3}$) or mass (nmol AA $min^{-1}\mu g^{-1}$) unit (Fang et al., 2016; Frezzini et al., 2022; Massimi et al., 2020a).

The OP^{DCFH} assay, which measures particle-bound ROS in terms of H_2O_2 equivalents, was adapted from the methodology of Huang et al. (2016). It is worth noting that most of the particle-bound ROS is unstable (Bates et al., 2019; Frezzini et al., 2022) and that the application of the assay on sampled PM filters only measures the more stable fraction of ROS. The process began with the preparation of the DCFH solution in the dark: 4.873 mg of 2′,7′-dichlorodihydrofluorescein diacetate (DCFH-DA) was dissolved in 5 mL of ethanol and mixed with 20 mL of 0.01 M NaOH for 30 min to promote deacetalization. Separately, the Horseradish Peroxidase (HRP) solution was prepared by dissolving 3.15 mg of HRP in 1 L of 25 mM phosphate buffer at pH 7.4. For the reaction, 1.5 mL of the water-extracted PM solution was combined with 5 mL of the HRP solution and with 125 μL of the prepared DCFH solution. This mixture was incubated for 5 min at 37 °C before being analyzed with a fluorescence detector (Jasco FP-920) at a 530 nm emission wavelength (427 nm excitation). The resulting fluorescence intensity was converted to OPv^{DCFH} (nmol H_2O_2 m^{-3}) or OPm^{DCFH} (nmol H_2O_2 μg^{-1}) values using a calibration curve derived from standard H_2O_2 solutions (Frezzini et al., 2022; Huang et al., 2016; Massimi et al., 2020a).

The minimum detection limit (MDL) for each analyte (Table 1) was determined as the average of ten replicate blank determinations plus three times their standard deviation (SD).

2.3. Positive matrix factorization

Source apportionment of PM_{10} was carried out using the PMF receptor model; a selection of 28 variables was made from the suite of analyzed species: PM_{10}, OC, EC, LVGSN, Ca^{++}, Cl^-, K^+, Mg^{++}, Na^+, NH_4^+, NO_3^-, $SO_4^=$, Al, As, Co, Cr, Cu, Fe, La, Mn, Mo, Ni, Pb, Sb, Sn, Sr, Ti, and V. A preliminary mass closure assessment was performed before PMF analysis to verify the internal consistency of the chemical dataset used as model input.

Uncertainties were estimated following established approaches: for concentrations below the MDL, uncertainties were calculated according to Polissar et al. (1998), while for concentrations above the MDL, the equation-based method described by Norris et al. (2014) was applied. These approaches inherently account for both analytical uncertainty and variability associated with measurements close to the detection limit. No additional uncertainty scaling was applied to specific tracer species, in order to preserve the objectivity of the dataset.

The selection of input variables was based on three main criteria: (i) compliance with the signal-to-noise (S/N) criterion (Paatero and Hopke, 2003), excluding variables with S/N < 2 or with more than 20% of values below the MDL; (ii) their established ability to trace emission sources (Massimi et al., 2022a, 2022b, 2024); and (iii) the results of iterative sensitivity tests aimed at optimizing source identification and model interpretability. These tests involved the systematic reduction or substitution of variables to identify the combination that best resolved known emission sources. Consequently, all selected variables were classified as “strong”, except for PM_{10} mass concentration, which was treated as a “weak” variable representing the total mass constraint.

Table 1
MDL and descriptive statistics for PM_{10} mass and chemical components concentration, OP^{DTT}, OP^{AA}, and OP^{DCFH}.

	UoM	MDL	Mean	*Std. Dev.*	Median	Min	Max
PM_{10} Mass Concentration	μg m^{-3}	5.0	**27**	*17*	22	7.0	100
OC	μg m^{-3}	0.50	**7.7**	*7.4*	4.0	1.70	39
EC	μg m^{-3}	0.05	**0.92**	*0.71*	0.63	0.11	3.9
LVGSN	μg m^{-3}	0.01	**0.86**	*1.2*	0.19	<0.01	5.6
Ca^{++}	μg m^{-3}	0.50	**0.71**	*0.42*	0.67	<0.50	2.0
Cl^{-}	μg m^{-3}	0.10	**0.33**	*0.46*	0.18	<0.10	2.5
K^{+}	μg m^{-3}	0.03	**0.27**	*0.25*	0.16	<0.03	1.2
Mg^{++}	μg m^{-3}	0.05	**0.052**	*0.056*	0.035	<0.05	0.36
Na^{+}	μg m^{-3}	0.50	**0.34**	*0.38*	0.23	<0.50	2.3
NH_4^{+}	μg m^{-3}	0.05	**0.38**	*0.30*	0.31	<0.05	1.4
NO_3^{-}	μg m^{-3}	0.05	**0.38**	*0.39*	0.22	<0.05	2.1
SO_4 =	μg m^{-3}	0.05	**0.48**	*0.30*	0.41	0.060	1.9
Al	μg m^{-3}	0.030	**0.28**	*0.34*	0.18	0.044	2.6
As	ng m^{-3}	0.60	**0.36**	*0.20*	0.34	<0.60	1.1
Co	ng m^{-3}	0.10	**0.19**	*0.13*	0.16	<0.10	0.70
Cr	ng m^{-3}	1.00	**16**	*14*	12	<1.00	89
Cu	ng m^{-3}	1.00	**5.3**	*3.1*	4.4	<1.00	16
Fe	ng m^{-3}	10.0	**336**	*214*	290	51.0	1596
La	ng m^{-3}	0.10	**0.25**	*0.31*	0.18	<0.10	2.3
Mn	ng m^{-3}	0.50	**15**	*13*	12	1.60	117
Mo	ng m^{-3}	0.50	**19**	*22*	11	<0.50	105
Ni	ng m^{-3}	1.00	**6.7**	*5.3*	5.0	<1.00	29
Pb	ng m^{-3}	2.00	**4.3**	*2.7*	3.7	<2.00	14
Sb	ng m^{-3}	0.10	**0.51**	*0.37*	0.41	<0.10	2.1
Sn	ng m^{-3}	0.50	**2.6**	*2.0*	2.0	0.51	12
Sr	ng m^{-3}	1.00	**3.3**	*2.5*	2.4	<1.00	14
Ti	ng m^{-3}	1.00	**8.3**	*9.2*	6.0	<1.00	69
V	ng m^{-3}	1.00	**1.0**	*0.72*	0.78	<1.00	5.0
OPv^{DTT}	nmol DTT min^{-1} m^{-3}	0.010	**0.92**	*0.51*	0.88	0.044	2.1
OPv^{AA}	nmol AA min^{-1} m^{-3}	0.0040	**5.0**	*3.2*	4.8	0.053	13
OPv^{DCFH}	nmol H_2O_2 m^{-3}	0.0010	**0.11**	*0.14*	0.041	0.0016	0.57
OPm^{DTT}	nmol DTT min^{-1} μg^{-1}	0.24	**31**	*36*	17	0.38	205
OPm^{AA}	nmol AA min^{-1} μg^{-1}	0.10	**131**	*116*	113	1.1	707
OPm^{DCFH}	nmol H_2O_2 μg^{-1}	0.025	**4.7**	*7.7*	0.87	0.026	41

Source apportionment was performed using the receptor model according to the following equation:

$$x_{ij} = \sum_{k=1}^{p} G_{ik}F_{kj} + E_{ij}$$

where Xij is the measured mass fraction of species j in sample i, Gik represents the mass contribution of source k to sample i, Fkj is the fractional abundance of species j in source k, and Eij is the residual between the measured and modeled mass fraction of species.

The PMF solution is obtained by minimizing the objective function Q, defined as the sum of squared residuals weighted by their uncertainties, through an iterative process that adjusts the G and F matrices while imposing non-negativity constraints to ensure physically meaningful solutions. A detailed description of the PMF approach is available elsewhere (Paatero and Hopke, 2003; Paatero, 1999; Hopke et al., 2020). The analysis was performed using the U.S. EPA PMF version 5.0 software (Norris et al., 2014), implemented through the Multilinear Engine (ME-2) algorithm (Paatero, 1999). PMF solutions were explored in Q-robust mode, and the optimal number of factors was selected by considering both the Qrob/Qexp trend and the physical interpretability of the factor profiles. The final solution was obtained from 100 runs.

Model uncertainty and stability were assessed using bootstrap (BS), displacement (DISP), and bootstrap enhanced by displacement (BS-DISP) analyses, as implemented in the EPA PMF v5.0 software. Bootstrap analysis was performed using 30 runs, and factor mapping was used to evaluate the reproducibility of the identified sources (supplementary materials). DISP analysis was applied to all variables included in the model to assess rotational ambiguity. Model performance was further evaluated through the inspection of scaled residuals, which did not show significant systematic patterns, indicating a satisfactory agreement between measured and modeled concentrations. Higher uncertainty associated with selected species reflects their contribution from multiple sources and atmospheric processes, rather than instability of the PMF solution. A summary of BS, DISP, and BS-DISP results is reported in the supplementary materials.

2.4. Multi-linear regression

Source apportionment of OP was performed using the MLR model (Weber et al., 2018; In 't Veld et al., 2023). Assuming that the OP is linearly linked to the PM_{10} mass concentration due to the different sources, OP^{DTT}, OP^{AA}, and OP^{DCFH} were set as the dependent variables, and the source contributions obtained from the PMF analysis were set as the explanatory variables to have an independent estimate of the source contributions to OP. The MLR model was applied by retaining all PMF-identified sources as explanatory variables, without excluding those showing low, negative, or non-significant linear correlations. This was a deliberate modeling choice aimed at ensuring consistency across the different OP assays and preserving the physical interpretability of source contributions, rather than optimizing model performance through selective source removal.

Source apportionment of OP by MLR was performed on volume-normalized OP values (OPv^{DTT}, OPv^{AA}, and OPv^{DCFH}) after confirming very good collinearity with the respective mass-normalized OP (OPm^{DTT}, $R^2 = 0.78$; OPm^{AA}, $R^2 = 0.75$, and OPm^{DCFH}, $R^2 = 0.86$), whose time series over the whole monitoring period are reported in the supplementary materials. The MLR model was implemented using the linear regression tool of the XLSTAT software (Addinsoft Lumivero, France), applying an ordinary least squares (OLS) approach and constraining the intercept to zero, according to Cesari et al. (2019), using the following equation:

$$OP = (G_i * \beta_i) + \varepsilon$$

where OP is a vector of the size of the observed OP (OPv^{DTT}, OPv^{AA}, and

OPv^{DCFH}); G is the matrix of the mass contribution of the PM_{10} sources; β_i is the intrinsic OP of the source, and ε is the residual term that accounts for the misfit between the observations and the model.

Residuals were inspected through visual analysis of residuals versus fitted values plots to assess the presence of heteroscedasticity (supplementary materials). No systematic patterns or funnel-shaped distributions were observed, suggesting that the assumption of homoscedasticity was reasonably satisfied. Analysis of variance (ANOVA, 95% confidence interval) was performed using a one-way ANOVA test. Results were considered statistically significant at $p < 0.05$.

3. Results and discussion

3.1. Source apportionment

PM_{10} mass concentration shows a mean value of 27 μg m^{-3} over the entire monitoring year, with pronounced daily variability (Fig. 4; Table 1), ranging from 7 μg m^{-3} during the summer period up to 100 μg m^{-3} in winter. The highest concentrations occur during the coldest months (i.e. January, February, November, and December), with a mean winter PM_{10} mass concentration of 39 μg m^{-3}. Conversely, the spring and summer months (March through October) are characterized by substantially lower mean PM_{10} mass concentration (21 μg m^{-3}), showing only two daily episodes exceeding 50 μg m^{-3} (Fig. 4). This strong fluctuation suggests that meteorological factors, such as atmospheric stability and boundary layer height (Ferrero et al., 2012; Guerrini, 2012; Moroni et al., 2013; Tositti et al., 2020), as well as the seasonal intensity of key emission sources, are the primary drivers of the overall PM_{10} mass concentration (Massimi et al., 2020a, 2020b; 2020c; 2022b). Table 1 reports the experimentally measured chemical species used as input variables for the PMF model, whereas Table 2 presents the PMF-derived source contributions. The standard deviation reported in Tables 1 and 2 represents the variability of each parameter within the dataset, reflecting temporal fluctuations associated with changes in atmospheric conditions and in the strength of emission sources.

Source apportionment via PMF analysis identified 7 main emission sources of PM_{10} (Fig. 3): (I) biomass burning for domestic heating, mainly traced by OC, EC, LVGSN and K^+; (II) vehicular traffic, including exhaust emissions traced by OC and EC as well as non-exhaust emissions from both vehicular and rail traffic, mainly traced by Cu, Fe, Mn, Sb and Sn; (III) one steel plant source primarily releasing Co, Cu, Cr, Ni and Pb; (IV) a second steel plant PM emission mainly characterized by As and Mo; (IV) soil dust represented by crustal elements (Al, Fe, La, Sr, Ti and V); (VI) sea spray transporting the main sea salt ions (Cl^-, Mg^{++} and Na^+) to the study area; and (VII) secondary inorganic species, dominated by ammonium (NH_4^+) nitrate (NO_3^-) and sulphate ($SO_4^=$).

The selection of the 7-factor solution represents the best compromise between statistical performance and physical interpretability. Solutions with fewer factors resulted in partial merging of distinct emission sources (e.g. traffic and industrial emissions), while higher-factor solutions led to over-splitting and less meaningful profiles. The chosen solution provides chemically coherent and physically interpretable source profiles, consistent with the known emission sources in the study area (Massimi et al., 2020b, 2022b). Error estimation analyses (BS, DISP, and BS-DISP), reported in the supplementary materials, indicate that most species are associated with relatively narrow confidence intervals, while the variability observed for selected species (e.g. OC, EC, $SO_4^=$, NH_4^+) reflects their multi-source origin and atmospheric processing rather than instability of the model. Rotational ambiguity was found to be limited, as confirmed by DISP analysis, which did not produce significant changes in factor profiles. The BS-DISP results further support the robustness of the solution when both resampling and rotational uncertainties are considered. In addition, the bootstrap factor mapping shows a high reproducibility of the solution, with most factors consistently mapped in all bootstrap runs and no unmapped factors observed (supplementary materials). Only minor mixing is observed for the traffic-related factor, which is expected given the partial overlap between combustion and non-exhaust emissions. It is worth noting that no external constraints were applied during PMF modeling. This choice was made to preserve a fully data-driven solution and avoid introducing a priori assumptions. As a consequence, some degree of mixing between sources (e.g. secondary inorganic components within combustion-related factors) may occur, reflecting the intrinsic complexity of PM_{10}. Overall, the combination of statistical diagnostics, error estimation analyses, and the physical consistency of the identified source profiles supports the robustness and reliability of the PMF solution.

Table 2
Descriptive statistics for PM_{10} source contributions identified by PMF.

	UoM	Mean	*Std. Dev.*	Median	Min	Max
Biomass Burning	μg m^{-3}	**13**	*13*	9.4	0.052	65
Vehicular Traffic	μg m^{-3}	**5.5**	*3.4*	4.9	0.33	16
Steel Plant 1	μg m^{-3}	**1.7**	*1.7*	1.2	0.031	9.9
Steel Plant 2	μg m^{-3}	**1.4**	*1.6*	0.72	0.011	6.9
Soil Dust	μg m^{-3}	**5.2**	*6.8*	3.5	0.063	49
Sea Spray	μg m^{-3}	**1.3**	*1.9*	0.75	0.0010	12
Secondary Inorganics	μg m^{-3}	**3.8**	*3.1*	3.1	0.048	18

3.1.1. Source profiles

The biomass burning source is primarily characterized by OC (52%), EC (47%), LVGSN (85%), and K^+ (57%). The EC/OC, LVGSN/OC, and K^+/LVGSN diagnostic ratios observed in this profile fall within the range of several biomass burning profiles available in SPECIEUROPE, the European repository for chemical profiles of PM sources (Pernigotti et al., 2016). LVGSN and K^+ are widely recognized, respectively, as the most dominant organic and inorganic components released in fine smoke PM during wood burning. LVGSN, a monosaccharide anhydride, is known to be released during the pyrolysis of cellulose at temperatures exceeding 300 °C (Chow et al., 2007; Simoneit et al., 2004), while K^+ is typically found at relatively high concentrations in the wood and pellet ashes produced by domestic heating systems (Liu et al., 2017; Sullivan et al., 2008). These components were already confirmed as selective tracers of biomass burning in the Terni basin (Massimi et al., 2020b, 2020c). It is worth noting that the concentrations of LVGSN and K^+ (Table 1) are significantly higher than those measured in other study areas in Central Italy (Massimi et al., 2022a, 2025; Perrino et al., 2020), reflecting the strong contribution from biomass burning in the Terni basin. Additionally, a significant portion of NO_3^- (28%) was found to be associated with this source, a finding consistent with the results of other studies (Behera and Balasubramanian, 2014; Simpson et al., 2002; Song and Liu, 2023). However, it is important to note that the relatively high NO_3^- contribution attributed to biomass burning may stem from an overestimation by the PMF model. The model likely struggled to correctly separate the NO_3^- of the secondary inorganic component of ammonium nitrate from the biomass burning contribution. As both sources are prevalent in winter and show very similar daily variability, this could have resulted in a misestimation of the NO_3^- partitioning between the two identified sources. This limitation is not specific to the present dataset but has been widely reported in previous PMF applications, particularly in wintertime conditions when biomass burning and secondary inorganic aerosol formation exhibit strong temporal co-variation. Several studies have shown that nitrate associated with ammonium nitrate formation may be partially misallocated to combustion-related sources due to collinearity in their temporal trends

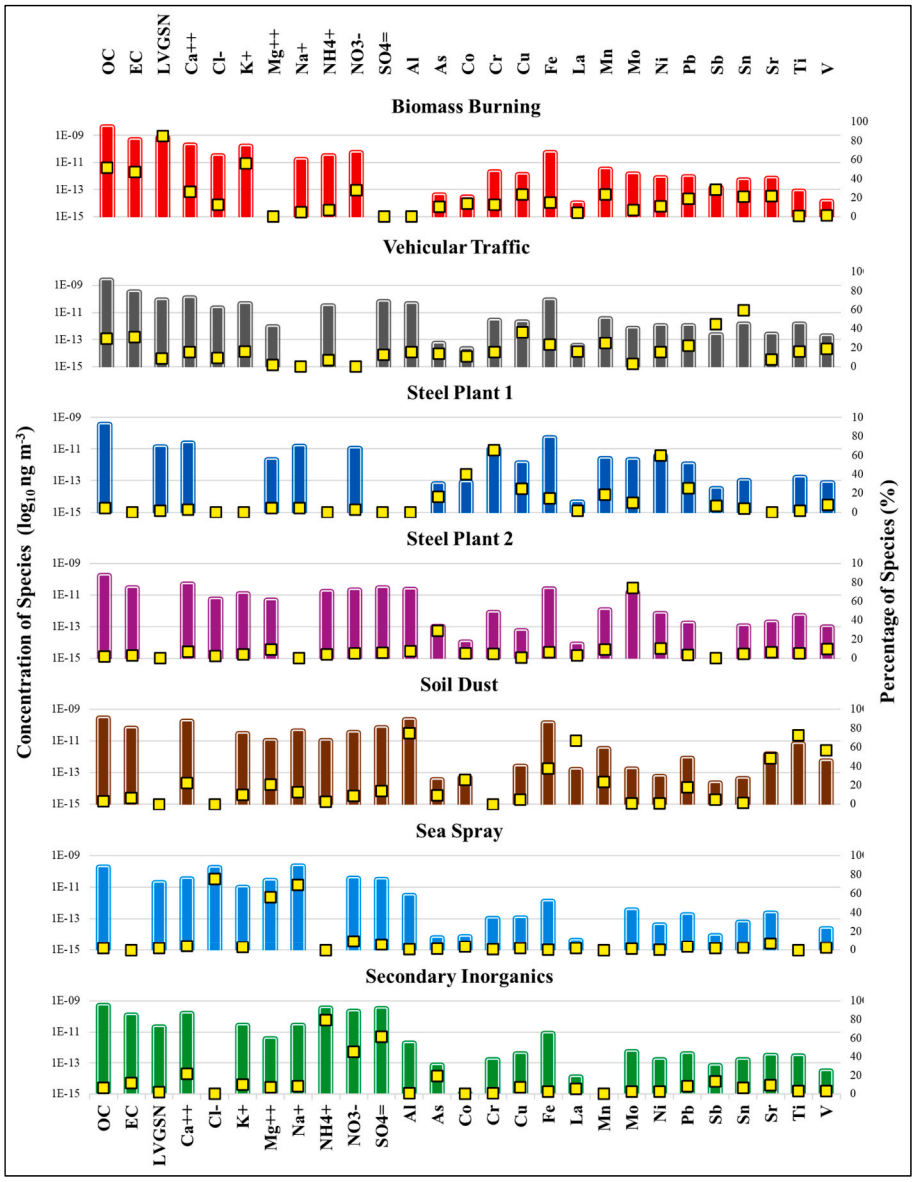

Fig. 3. Chemical profiles of the sources identified by the PMF analysis. Colored bars represent $\log_{10}$ normalized average species concentration (ng m^{-3}) while the yellow dots represent the average species percentage (%) across sources. (For interpretation of the references to colour in this figure legend, the reader is referred to the Web version of this article.)

and shared seasonal patterns (Belis et al., 2019; Crippa et al., 2014; Lanz et al., 2008). Under such conditions, even well-constrained PMF solutions may struggle to fully disentangle secondary nitrate from primary combustion contributions. Therefore, the relatively high NO_3^- fraction attributed to biomass burning in this study should be interpreted with caution and considered as indicative of mixed or overlapping source influences rather than a purely primary emission signal. Finally, this profile exhibits lower abundances (20-30%) of potentially toxic elements (PTEs), such as Cu, Mn, Sb, and Sn, raising concern regarding potential health risks associated with the inhalation of these components. This concern is strongly supported by a recent study, which demonstrated the elevated contribution from biomass burning to the carcinogenic risk associated with exposure to these PTEs in PM_{10} throughout the Terni basin (Massimi et al., 2022b).

The vehicular traffic source includes both exhaust and non-exhaust traffic emissions because the PMF model was unable to disaggregate the two components due to the unavailability of selective tracers for exhaust emissions. The exhaust traffic is mainly represented by OC (30%) and EC (32%), while the non-exhaust component is primarily characterized by several PTEs, such as Cu (36%), Fe (23%), Mn (25%), Sb (45%), and Sn (59%). The EC/OC, Sb/Cu, and Sb/Sn ratios of this chemical profile fall within the variability ranges of the diagnostic ratios of different traffic profiles available in SPECIEUROPE (Pernigotti et al., 2016). Cu, Fe, Mn, Sb, and Sn are widely recognized as tracers of PM emissions from vehicle brake wear and abrasion of rolling stock from railway traffic (Amato et al., 2009; Namgung et al., 2016; Querol et al., 2012). Several studies carried out in the Terni basin confirmed their selectivity as tracers of brake dust released by both vehicular and rail traffic (Massimi et al., 2020a, 2020b, 2022). High concentrations of PTEs from non-exhaust traffic are implicated in the health risks associated with PM inhalation (Kam et al., 2013).

In the Terni basin, brake dust was identified as a relevant contributor to the non-carcinogenic risk associated with inhalation exposure of PTEs in PM_{10}, especially near the train station (Massimi et al., 2022b). While considerable progress has been made in reducing exhaust emissions from vehicles, the regulation and mitigation strategies for non-exhaust traffic remain largely undeveloped, even though brake dust has been shown to induce oxidative stress due to its content of various

redox-active chemical species (Amato et al., 2009; Happo et al., 2010; Vaccarella et al., 2025b).

The first identified steel plant source is primarily characterized by Co (40%), Cu (25%), Cr (65%), Ni (60%), and Pb (25%), while the second steel plant emission is mainly represented by As (29%) and Mo (74%). The Ni/Cr and Ni/Mo ratios are comparable with the variability range of several diagnostic ratios of steel plant profiles available in SPECIEUROPE. As, Co, Cu, Cr, Mo, Ni, and Pb are PTEs used as the main components of stainless steel or to increase the steel toughness, ductility, and corrosion resistance (Taiwo et al., 2014; Owoade et al., 2015;Expósito et al., 2025), and were already effectively used in recent studies to trace the steel plant emissions in the Terni basin (Massimi et al., 2020a, 2020b, 2022). The two chemical profiles are likely associated with different PM_{10} emissions from the major processes occurring in the hot and cold areas of the industry (e.g. hot or cold rolling, abrasion, brushing, polishing, transport of rolled steel or steel slag), releasing PM with different size distribution, solubility and PTEs content (Cusano et al., 2025; Massimi et al., 2020a, 2020b, Massimi et al., 2022a;Massimi et al., 2022b). Although a direct comparison with source-specific emission profiles from the steel plant was not possible in the present study, ongoing high spatial resolution receptor modelling investigations within and around the industrial area are expected to provide process-specific chemical fingerprints, enabling a more detailed attribution of the PMF-derived steel plant factors to distinct emission sources. It is worth noting that the steel plant has been identified as the main contributor to both carcinogenic and non-carcinogenic inhalation risks due to PTEs in PM_{10} in the Terni basin, especially in the area surrounding the industry (SIN of Terni-Papigno), indicating potential health risks for residents in the nearby areas (Massimi et al., 2022b). Further studies are needed to clarify the main steel plant processes releasing PTEs in PM_{10} and their dispersion over the study area.

The soil dust component is represented by crustal elements, such as Al (75%), Fe (38%), La (67%), Sr (48%), Ti (72%), and V (57%), which proved to be very robust tracers of mineral dust in several studies (Bencharif-Madani et al., 2019; Massimi et al., 2022b; Perrino et al., 2020; Soleimanian et al., 2019). The Al/Fe and Al/Ti ratios fall within the range of numerous diagnostic ratios for crustal dust profiles present in SPECIEUROPE. It is important to note that the species within this chemical profile can be attributed not only to dust originating from the erosion and resuspension of local crustal material but also to PM_{10} transported from remote regions, such as dust incursion events from the North African desert regions (Linares et al., 2021; Massimi et al., 2022a, 2024; Perez et al., 2008). To investigate this transport, the Dust Regional Atmospheric Model (DREAM8) forecast was used to analyze the air mass trajectories.

The sea spray source is characterized by high contributions from Cl^- (75%), Na^+ (69%), and Mg^{++} (56%) and closely resembles the composition of sea salt (Seinfeld and Pandis, 2006). The Cl^-/Na^+ and Mg^{++}/Na^+ ratios are fully within the range of marine aerosol profiles in SPECIEUROPE. Although the Terni basin is quite far from coastal marine zones, sea salt ions can be transported to the study area due to the potential for long-range transport of marine aerosols, which can extend up to 1100 km inland (May et al., 2018).

Finally, the secondary inorganic component is represented by ammonium nitrate and sulphate, which are formed in the atmosphere from gaseous precursors (i.e., NH_3, NO_x, and SO_2), and is thus characterized by NH_4^+ (79%), NO_3^- (46%), and $SO_4^=$ (61%). In winter, lower temperatures and increased humidity facilitate the formation of ammonium nitrate, which is often the prevailing compound. In contrast, ammonium sulphate prevails in summer as a result of enhanced photochemical activity that increases the oxidation rate of SO_2 to sulphuric acid and its condensation into new ammonium sulphate particles (Amato et al., 2016).

3.1.2. Source contributions to PM_{10}

The overall PM_{10} source apportionment was very effective, showing an R^2 of 0.95 between measured and PMF-modeled PM_{10} (supplementary materials) with only 7% of the measured PM_{10} mass concentration unreconstructed (unknown) by the PMF model (Fig. 4).

Time series of daily source contributions to the PM_{10} mass concentration measured over the 2022 monitoring year in the Terni basin reveal a clear dominance of a few sources and strong seasonal variability in their contributions to PM_{10}. The comparison between measured and PMF-modeled PM_{10} time series is reported in the supplementary materials.

Biomass burning is notably the major PM_{10} source, contributing on average 29% to the overall PM_{10} mass concentration (Fig. 4), with annual mean values of 8 $\mu g\ m^{-3}$. This source exhibits a strong seasonal dependence, being the dominant contributor during the coldest months when home biomass heating is frequently used. Specifically, the winter period, spanning from January to February and from November to December, shows a mean contribution from biomass burning of 20 $\mu g\ m^{-3}$, with the highest daily contribution of as much as 65 $\mu g\ m^{-3}$ on January 26, 2022. Even though, as discussed, this source may be somewhat overestimated by the PMF, the significant contribution from domestic biomass heating highlights the necessity for targeted interventions during colder months to mitigate biomass combustion and its associated pollutants. This result is in line with previous studies carried out in Central Italy (Massimi et al., 2022a, 2022b, 2024, 2025) and is further supported by recent work combining emission data and receptor modelling, confirming the dominant role of domestic biomass burning in PM_{10} pollution (Marinelli et al., 2026).

Vehicular traffic also contributes considerably (20%) to the overall PM_{10} mass concentration and shows a generally consistent pattern throughout the year, with an average concentration of 5 $\mu g\ m^{-3}$. A noticeable increase in traffic contribution occurred towards the end of the year. This likely results from enhanced atmospheric stability typical of the winter season and increased vehicle usage during the pre-Christmas period. This pattern highlights the persistent impact of exhaust and non-exhaust vehicular emissions on air quality, with temporary exacerbations during periods of heightened activity, necessitating sustained traffic management and emission control strategies.

PM_{10} emission from the steel plant is quite limited; the two identified steel plant sources contribute together on average 10% of the overall PM_{10} mass concentration. Both contributions remain relatively constant throughout the year, indicating continuous industrial activity with stable emission rates.

Soil dust contributes notably to the PM_{10} mass concentration (17%). This source displays a seasonal increase during the spring and summer months (March through October), when it reaches values of 15 $\mu g\ m^{-3}$ due to enhanced soil dust resuspension in the atmosphere under drier conditions. The two occasional peaks, which occurred from 25th June to 3rd July and on 18th August (Fig. 4), are attributed to desert dust events, confirmed by the DREAM8 model (supplementary materials). Conversely, sea spray contribution is very low (4%) due to the distance of the Terni basin from the Italian coastal areas, and is fairly constant throughout the entire measurement year. A minor increase occurred from 27th September to 1st October due to greater advections of marine aerosol from the Tyrrhenian coast, as also demonstrated by the DREAM8 model.

Finally, secondary inorganic species contribute on average 13% to the PM_{10} mass concentration, with mean annual values of 3.5 $\mu g\ m^{-3}$, and show the highest contribution on 26th January (6 $\mu g\ m^{-3}$). This date coincided with the peak contribution from biomass burning and likely reflects wintertime conditions characterized by reduced atmospheric dispersion and low temperatures, which favor both the accumulation of combustion-related emissions and the formation and persistence of secondary inorganic aerosol, particularly ammonium nitrate.

3.1.3. Source contributions to OP

Source apportionment of OP was performed using MLR based on an OLS approach; results are summarized in Fig. 5 (standardized

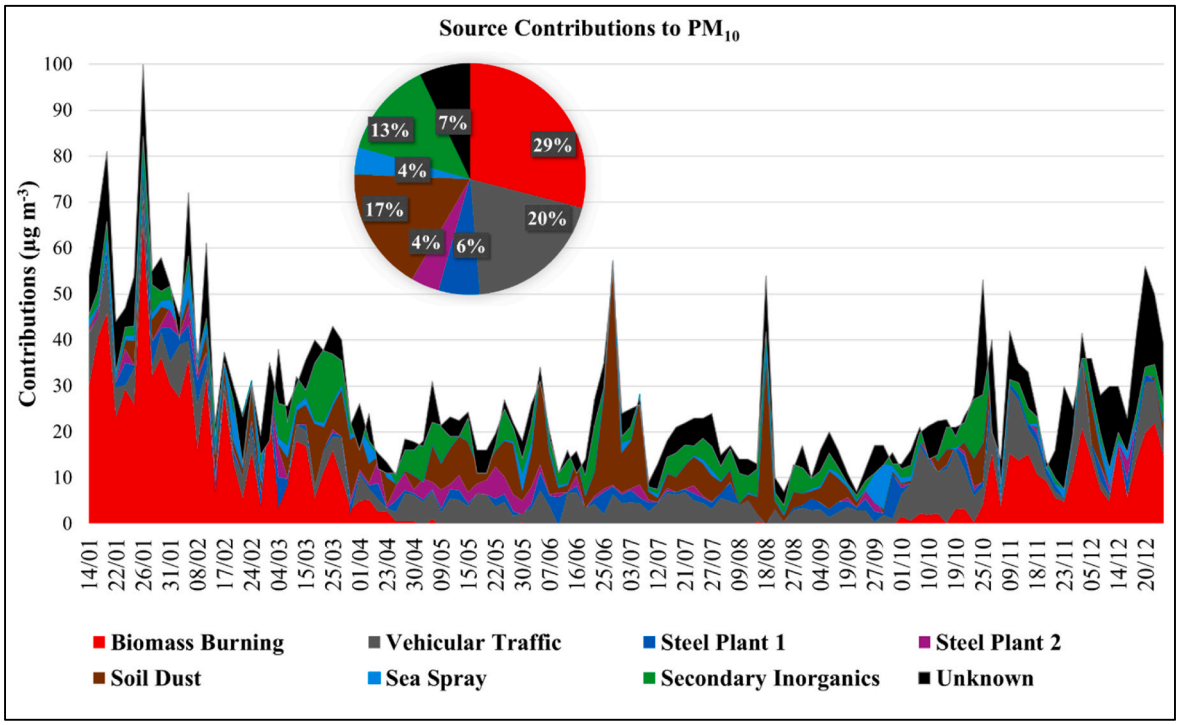

Fig. 4. Time series of daily source contributions to the PM_{10} mass concentration measured over the 2022 monitoring year in the Terni basin, along with the pie chart representing the average percentage (%) source contributions to PM_{10} mass concentration.

coefficients) and Fig. 6 (source contributions). Residuals versus fitted values plots (supplementary materials) did not reveal any systematic structures or heteroscedastic patterns, indicating approximately constant variance and supporting the validity of the OLS assumptions and the robustness of the regression model.

Overall, the different OP assays show distinct source-specific responses, reflecting their intrinsic chemical selectivity. The observed differences should be interpreted considering both the adopted modeling strategy and the nature of OP measurements. The decision to retain all PMF-derived sources in each MLR model ensures comparability and physical consistency (section 2.5) and enables a direct comparison among assays, preserving the full set of source contributions. Accordingly, no sources were excluded based on low, non-significant, or negative regression coefficients, allowing a comprehensive evaluation of how each source influences each OP metric within a unified framework. This approach prioritizes interpretability and comparability over predictive performance; therefore, a lower predictive capability and a higher fraction of unexplained variability are expected, particularly for assays less directly linked to the PMF-resolved sources. Rather than representing a limitation, this reflects the intrinsic complexity of OP, which is governed by the combined effects of multiple redox-active species. These species may interact through synergistic or antagonistic mechanisms and are further influenced by atmospheric aging and secondary photochemical processes (Ngoc Thuy et al., 2024; Pietrogrande et al., 2022b; Vaccarella et al., 2025). Consequently, the relationship between PM sources and OP is not strictly linear, and linear models can only partially capture this variability. Within this context, the lower predictive performance observed for some assays should be interpreted as a consequence of their chemical selectivity and the non-linear nature of the processes driving OP. These findings suggest that future source apportionment studies may benefit from the application of non-linear modeling approaches better suited to represent the complex interactions among PM components and their oxidative properties.

The MLR model shows strong performance for OPv^{DTT}, with a high agreement between measured and modeled values (Fig. 5A) and only 11% of unexplained variability (Fig. 6A). OPv^{DTT} is mainly driven by biomass burning and vehicular traffic, with high standardized coefficients (0.48 and 0.21, respectively) and contributions of 36% and 24%. Biomass burning reflects the influence of combustion-derived organics, while traffic highlights the role of metal-rich emissions (Amato et al., 2016; Massimi et al., 2024, 2025). This behavior is consistent with the known sensitivity of the OP^{DTT} assay to both transition metals and redox-active organic compounds such as quinones (Charrier and Anastasio, 2012; Massimi et al., 2020a; Vimukthi et al., 2025). Previous studies have consistently linked OP^{DTT} to combustion-related emissions, although the relative importance of individual sources varies depending on site characteristics and PM size fraction (Serafeim et al., 2023; Shen et al., 2022; Simonetti et al., 2018; Verma et al., 2015). Such variability has been attributed to differences in the abundance of redox-active organics and metals, as well as to synergistic or antagonistic interactions among PM components (Pietrogrande et al., 2022b; Ngoc Thuy et al., 2024; Vaccarella et al., 2025).

Additional significant contributions ($p < 0.05$) are associated with secondary inorganic species and the "Steel Plant 2" source, suggesting that the PMF model captures the main components influencing OP^{DTT}. This also indicates a potential role of industrial emissions in the oxidative properties of PM_{10}. Although secondary inorganic species (e.g. ammonium sulphate and nitrate) are generally considered to have low intrinsic redox activity, several studies have reported associations with OP, despite unclear mechanisms (Szigeti et al., 2015; Chen et al., 2022; Fadel et al., 2023; in't In 't Veld et al., 2023; Grange et al., 2022; Massimi et al., 2024). Recent experimental evidence (Vernocchi et al., 2025) suggests that these species may indirectly enhance OP through synergistic effects, for example, by modifying aerosol acidity and the solubility or redox cycling of transition metals. Therefore, the contribution of the secondary inorganic factor should be interpreted as a proxy of aged or internally mixed aerosol rather than a direct redox-active source. Overall, OP^{DTT} can be considered an integrative proxy of PM oxidative potential, influenced by both primary and secondary sources, in agreement with previous studies (Cesari et al., 2019; Daellenbach et al., 2020; Serafeim et al., 2023; Weber et al., 2021).

In contrast, the MLR model shows lower predictive capability for

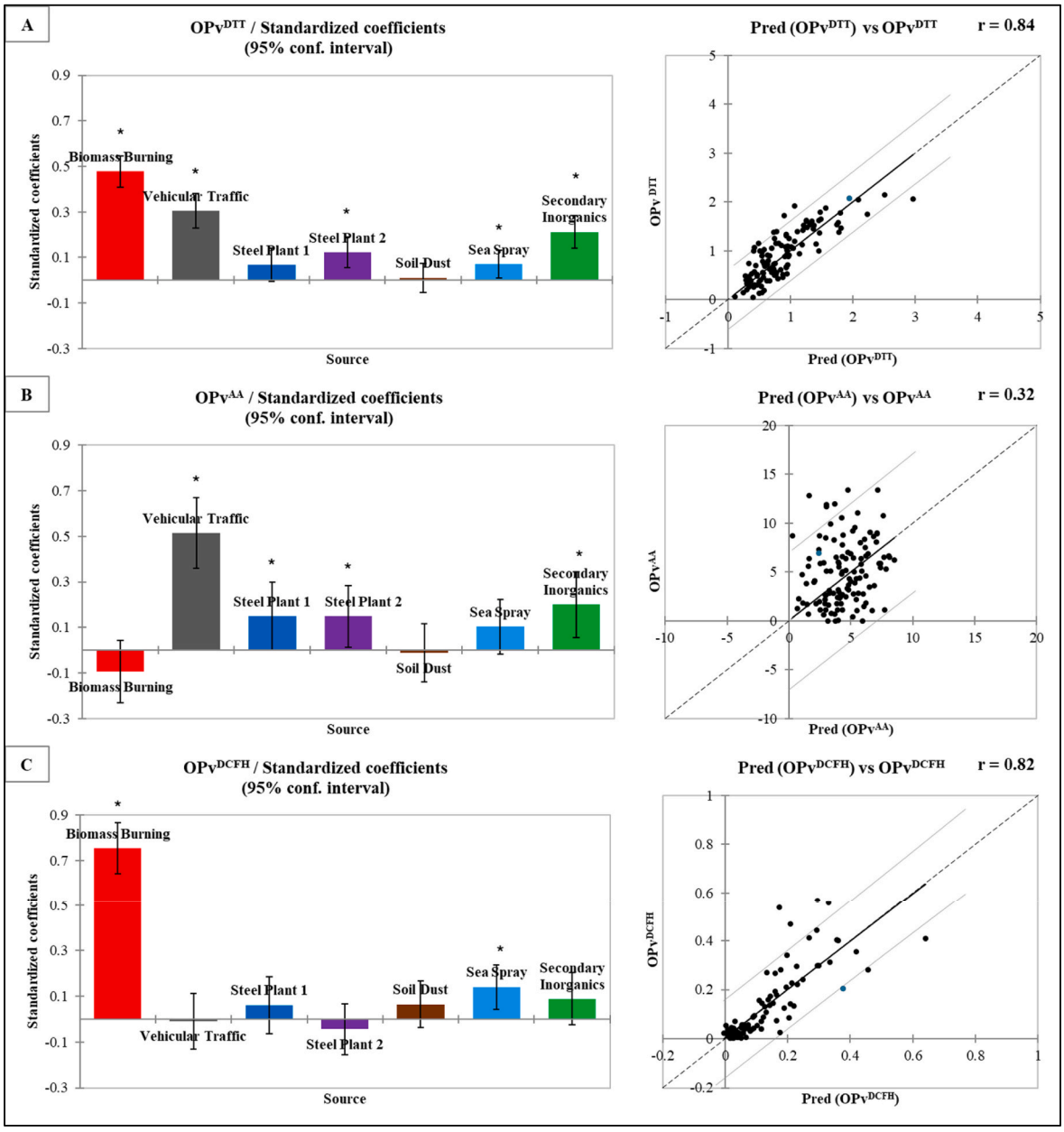

Fig. 5. Standardized coefficient plots representing OPv^{DTT} (panel A), OPv^{AA} (panel B), and OPv^{DCFH} (panel C) for each identified source contribution, together with the corresponding Pearson correlation coefficients (r) between measured and modeled OP values. Error bars represent 95% confidence intervals. Statistically significant coefficients are indicated by * ($p < 0.05$), based on analysis of variance (ANOVA). Scatter plots show the relationship between predicted and observed OP values, with the dashed line representing the 1:1 relationship and the solid line indicating the linear fit.

OPv^{AA}, as indicated by lower Pearson correlation coefficient (Fig. 5B) and a higher fraction of unexplained variability (36%; Fig. 6B). This suggests that the PMF factors do not fully resolve the specific chemical drivers of this assay. Vehicular traffic is identified as the dominant contributor to OPv^{AA} (43%; Fig. 6B) with a significant contribution ($p < 0.05$) and the highest standardized coefficient (0.52). This finding is consistent with the well-established sensitivity of the OP^{AA} assay to transition metals, particularly Cu and Fe (Bates et al., 2019; Charrier and Anastasio, 2012; Massimi et al., 2024; Molina et al., 2020; Pietrogrande et al., 2022), which are abundant in non-exhaust traffic emissions such as brake wear (Amato et al., 2009; Di Martino et al., 2026; Massimi et al., 2022b; Namgung et al., 2016; Pant and Harrison, 2013). Conversely, biomass burning shows no significant contribution to OP^{AA}, with a slightly negative coefficient (Fig. 5B). Although this may appear counterintuitive, it is consistent with the intrinsic selectivity of the assay, which is not responsive to the fine organic fraction typically emitted by biomass combustion. This interpretation is further supported by previous OP measurements of size-segregated PM (Massimi et al., 2020a; Simonetti et al., 2018), where OP^{AA} is predominantly associated with the coarse fraction, characteristic of mechanically generated particles rather than combustion-derived fine particles (Amato et al., 2016; Canepari et al., 2019; Daellenbach et al., 2020; Pant and Harrison, 2013). However, it is important to note that several studies conducted in different European and non-European contexts have reported a significant contribution of biomass burning to OP^{AA} (Dominutti et al., 2023; Fadel et al., 2023; Ngoc Thuy et al., 2024; Weber et al., 2021), in some cases identifying biomass burning as the dominant OP^{AA} source. These apparent discrepancies highlight that the OP^{AA} response cannot be interpreted solely based on source type but rather depends on the specific chemical composition of emissions and atmospheric processing. In

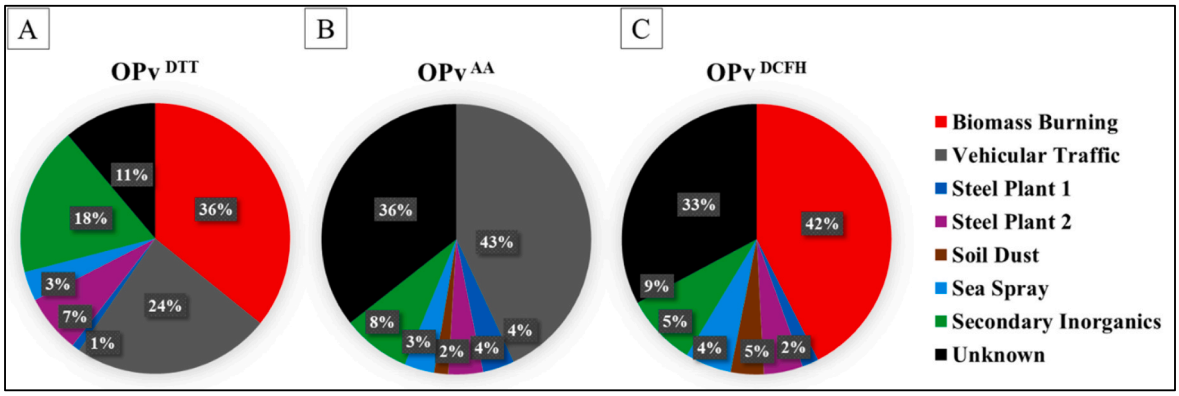

Fig. 6. Average percentage source contribution to OPv^{DTT} (panel A), OPv^{AA} (panel B), and OPv^{DTT} (panel C).

particular, biomass burning emissions may contribute to OP^{AA} when enriched in redox-active species such as metal-containing ash, oxygenated organic compounds, or humic-like substances, or when aging processes enhance the oxidative reactivity of emitted particles (Bates et al., 2019; Pietrogrande et al., 2022a; Vaccarella et al., 2025; Øvrevik, 2019). Therefore, the absence of a positive biomass burning contribution to OP^{AA} in the present study likely reflects site-specific emission characteristics and the predominance of traffic-related transition metal sources (Massimi et al., 2020a, 2022.

Biomass burning is instead identified as the main contributor to OPv^{DCFH}, with a significant contribution ($p < 0.05$) and a high standardized coefficient (0.75), accounting for 42% of the total OPv^{DCFH}. This behavior reflects the sensitivity of the OP^{DCFH} assay to particle-bound ROS and oxidative species generated during incomplete combustion processes. This result is consistent with previous studies showing that OP^{DCFH} is particularly responsive to combustion-derived particles and secondary ROS formation, often highlighting a stronger association with biomass burning compared to OP^{AA} (Daellenbach et al., 2020; Dominutti et al., 2023; Massimi et al., 2020a, 2024, 2025). The MLR model shows great predictive capability for OPv^{DCFH} as indicated by a high Pearson correlation coefficient (Fig. 5C). However, a substantial fraction of unexplained variability (33%; Fig. 6C) remains, likely reflecting the intrinsic limitations of source-based apportionment for this assay. Indeed, OP^{DCFH}, which targets particle-bound ROS, cannot be fully reconstructed using only PMF-derived emission sources, as ROS are influenced not only by primary PM composition but also by secondary photochemical formation processes in the atmosphere. Furthermore, since OP measurements are performed on water extracts of filter-collected PM with daily resolution, a significant fraction of highly reactive ROS may decay prior to analysis (Bates et al., 2019; Frezzini et al., 2022), leading to an underestimation of their contribution to the measured OP^{DCFH}.

Results from OP source apportionment are consistent with the temporal trends of volume-normalized (OPv) and mass-normalized (OPm) values (supplementary materials), which provide an indirect representation of the intrinsic OP of the different sources. The comparison between OPv and OPm metrics allows the assessment of source-specific oxidative activity.

Overall, biomass burning and traffic emerge as the main drivers of OP, although their relative contributions depend strongly on the assay considered. OP^{DTT} and OP^{DCFH} are primarily associated with combustion sources, while OP^{AA} is dominated by traffic emissions. These results are consistent with recent literature (Cesari et al., 2019; Daellenbach et al., 2020; Dominutti et al., 2023; Massimi et al., 2024, 2025). Moreover, previous studies conducted in the Terni basin support these observations (Massimi et al., 2020a). Higher OP^{AA} values were reported near traffic-dominated sites (e.g. busy roads, railway), while OP^{DTT} showed elevated levels in residential areas during winter. In addition, size-resolved analyses demonstrated that OP^{AA} is mainly associated with coarse particles, whereas OP^{DTT} and OP^{DCFH} are more strongly linked to fine combustion-derived particles, further supporting the source-specific behavior observed here.

More generally, the comparison with recent OP source apportionment studies highlights that the relative importance of sources (e.g. biomass burning, traffic, industrial emissions) varies substantially across geographical areas, reflecting differences in emission profiles, atmospheric processing, and particle composition (Daellenbach et al., 2020; In 't Veld et al., 2023; Vaccarella et al., 2025). This variability confirms that the combined use of multiple OP assays is essential to capture the full complexity of PM oxidative properties and to better link emission sources with potential health effects.

4. Conclusion

Source apportionment of PM_{10} in the urban-industrial hot spot of Terni provides relevant local-scale information to support air quality management strategies. In particular, the results of this study highlight the key role of winter biomass burning emissions in the Terni basin, suggesting that targeted mitigation measures may be effective not only for reducing PM_{10} mass concentrations in view of the targets set by the new Air Quality Directive 2024/2881/EU, but also for limiting the contribution of combustion-related sources to PM oxidative properties.

Source apportionment of OP revealed a marked differential sensitivity among the investigated assays. OP^{DTT} showed the most comprehensive response to multiple emission sources, including biomass burning, vehicular traffic, industrial emissions, and secondary components, suggesting its suitability as an integrative proxy of PM oxidative potential. OP^{AA} was predominantly associated with vehicular traffic, confirming its sensitivity to transition metals from non-exhaust emissions, while OP^{DCFH} was mainly driven by biomass burning, reflecting its sensitivity to combustion-related oxidative species. These differences highlight the importance of combining multiple OP assays to capture the source-specific variability of PM oxidative properties.

The application of MLR allowed a direct comparison with previous OP source apportionment studies and provided a consistent approach to evaluate the contribution of PMF-identified sources across the different assays. At the same time, the results highlight the complexity of OP responses, which depend on multiple interacting chemical components and processes. In this context, future studies may benefit from the integration of alternative modeling approaches capable of accounting for potential non-linear interactions.

Overall, the findings of this study demonstrate that OP source apportionment provides complementary information to PM mass-based analysis, improving the identification of emission sources associated with enhanced oxidative potential. The variability observed among OP assays further indicates that a multi-metric approach is necessary to better characterize the oxidative properties of PM and their relation to emission sources.

Declaration of generative AI and AI-assisted technologies in the writing process

During the preparation of this work the author(s) used ChatGPT AI in order to correct eventual English grammar errors and improve readability. After using this tool/service, the author(s) reviewed and edited the content as needed and take(s) full responsibility for the content of the published article.

Funding

This work was partially funded by the project 2024 RM124190EA13B276 (Principal Investigator Lorenzo Massimi), financed by Sapienza University of Rome.

CRediT authorship contribution statement

Lorenzo Massimi: Conceptualization, Data curation, Supervision, Writing – original draft, Writing – review & editing. **Alice Zara:** Data curation, Formal analysis, Writing – original draft. **Caterina Tiraboschi:** Data curation, Formal analysis. **Mara Galletti:** Conceptualization, Supervision. **Marco Vecchiocattivi:** Conceptualization, Supervision. **Silvia Canepari:** Conceptualization, Supervision, Writing – review & editing.

Declaration of competing interest

The authors declare that they have no known competing financial interests or personal relationships that could have appeared to influence the work reported in this paper.

Appendix A. Supplementary data

Supplementary data to this article can be found online at https://doi.org/10.1016/j.atmosenv.2026.122044.

Data availability

Data will be made available on request.

References

Abrams, J.Y., Weber, R.J., Klein, M., Samat, S.E., Chang, H.H., Strickland, M.J., et al., 2017. Associations between ambient fine particulate oxidative potential and cardiorespiratory emergency department visits. Environ. Health Perspect. 125 (10), 107008.

Adorno, S., Neri Serneri, S., 2009. Industria, Ambiente E Territorio. per Una Storia Ambientale Delle Aree Industriali in Italia. Il Mulino, pp. 1–366.

Al-Kindi, S.G., Brook, R.D., Biswal, S., Rajagopalan, S., 2020. Environmental determinants of cardiovascular disease: lessons learned from air pollution. Nat. Rev. Cardiol. 17 (10), 656–672.

Ali, Muhammad Ubaid, Liu, Guijian, Yousaf, Balal, Habib, Ullah, Abbas, Qumber, Munir, Mehr Ahmad Mujtaba, 2019. A systematic review on global pollution status of particulate matter-associated potential toxic elements and health perspectives in urban environment. Environ. Geochem. Health 41, 1131–1162.

Ali-Taleshi, Saleh, Mohammad, Feiznia, Sadat, Masiol, Mauro, 2022. Seasonal and spatial variations of atmospheric depositions-bound elements over Tehran megacity, Iran: pollution levels, PMF-based source apportionment and risks assessment. Urban Clim. 42, 101113.

Amato, F., Alastuey, A., Karanasiou, A., Lucarelli, F., Nava, S., Calzolai, G., Querol, X., 2016. AIRUSE-LIFE+: a harmonised PM speciation and source apportionment in five southern European cities. Atmos. Chem. Phys. 16 (5), 3289–3309.

Amato, F., Pandolfi, M., Viana, M., Querol, X., Alastuey, A., Moreno, T., 2009. Spatial and chemical patterns of PM10 in road dust deposited in urban environment. Atmos. Environ. 43 (9), 1650–1659.

Arias-Pérez, R.D., Taborda, N.A., Gómez, D.M., Narvaez, J.F., Porras, J., Hernandez, J.C., 2020. Inflammatory effects of particulate matter air pollution. Environ. Sci. Pollut. Control Ser. 27 (34), 42390–42404.

Ashrafi, K., Fallah, R., Hadei, M., Yarahmadi, M., Shahsavani, A., 2018. Source apportionment of total suspended particles (TSP) by positive matrix factorization (PMF) and chemical mass balance (CMB) modeling in Ahvaz, Iran. Arch. Environ. Contam. Toxicol. 75, 278–294.

Ayres, J.G., Borm, P., Cassee, F.R., Castranova, V., Donaldson, K., Ghio, A., et al., 2008. Evaluating the toxicity of airborne particulate matter and nanoparticles by measuring oxidative stress potential—a workshop report and consensus statement. Inhal. Toxicol. 20 (1), 75–99.

Barrington-Leigh, C., Baumgartner, J., Carter, E., Robinson, B.E., Tao, S., Zhang, Y., 2019. An evaluation of air quality, home heating and well-being under Beijing's programme to eliminate household coal use. Nat. Energy 4 (5), 416–423.

Bates, J.T., Fang, T., Verma, V., Zeng, L., Weber, R.J., Tolbert, P.E., et al., 2019. Review of acellular assays of ambient particulate matter oxidative potential: methods and relationships with composition, sources, and health effects. Environ. Sci. Technol. 53 (8), 4003–4019.

Behera, S.N., Balasubramanian, R., 2014. Influence of biomass burning on temporal and diurnal variations of acidic gases, particulate nitrate, and sulfate in a tropical urban atmosphere. Adv. Meteorol. 2014 (1), 828491.

Belis, C.A., Pikridas, M., Lucarelli, F., Petralia, E., Cavalli, F., Calzolai, G., et al., 2019. Source apportionment of fine PM by combining high time resolution organic and inorganic chemical composition datasets. Atmos. Environ. X 3, 100046.

Beloconi, A., Vounatsou, P., 2023. Revised EU and WHO air quality thresholds: where does Europe stand? Atmos. Environ., 120110

Bencharif-Madani, F., Ali-Khodja, H., Kemmouche, A., Terrouche, A., Lokorai, K., Naidja, L., Bouziane, M., 2019. Mass concentrations, seasonal variations, chemical compositions and element sources of PM10 at an urban site in Constantine, northeast Algeria. J. Geochem. Explor. 206, 106356.

Bi, X., Dai, Q., Wu, J., Zhang, Q., Zhang, W., Luo, R., et al., 2019. Characteristics of the main primary source profiles of particulate matter across China from 1987 to 2017. Atmos. Chem. Phys. 19 (5), 3223–3243.

Bălă, G.P., Răjnoveanu, R.M., Tudorache, E., Motişan, R., Oancea, C., 2021. Air pollution exposure—the (in) visible risk factor for respiratory diseases. Environ. Sci. Pollut. Control Ser. 28, 19615–19628.

Buiarelli, Francesca, Di Filippo, Patrizia, Pomata, Donatella, Riccardi, Carmela, Simonetti, Giulia, 2018. A rapid method for the determination of levoglucosan in NIST standard reference material 1649a by HPLC-MS/MS. Atmos. Environ. 195, 24–29.

Canepari, S., Astolfi, M.L., Catrambone, M., Frasca, D., Marcoccia, M., Marcovecchio, F., et al., 2019. A combined chemical/size fractionation approach to study winter/summer variations, ageing and source strength of atmospheric particles. Environ. Pollut. 253, 19–28.

Canepari, S., Cardarelli, E., Pietrodangelo, A., Strincone, M., 2006. Determination of metals, metalloids and non-volatile ions in airborne particulate matter by a new two-step sequential leaching procedure: part B: validation on equivalent real samples. Talanta 69 (3), 588–595.

Canepari, S., Perrino, C., Astolfi, M.L., Catrambone, M., Perret, D., 2009. Determination of soluble ions and elements in ambient air suspended particulate matter: Inter-technique comparison of XRF, IC and ICP for sample-by-sample quality control. Talanta 77 (5), 1821–1829.

Capelli, L., Sironi, S., Del Rosso, R., Céntola, P., Rossi, A., Austeri, C., 2011. Olfactometric approach for the evaluation of citizens' exposure to industrial emissions in the city of Terni, Italy. Sci. Total Environ. 409 (3), 595–603.

Cesari, D., Merico, E., Grasso, F.M., Decesari, S., Belosi, F., Manarini, F., et al., 2019. Source apportionment of PM2. 5 and of its oxidative potential in an industrial suburban site in South Italy. Atmosphere 10 (12), 758.

Charrier, J.G., Anastasio, C., 2012. On dithiothreitol (DTT) as a measure of oxidative potential for ambient particles: evidence for the importance of soluble transition metals. Atmos. Chem. Phys. 12 (5), 11317.

Chen, K., Xu, J., Famiyeh, L., Sun, Y., Ji, D., Xu, H., et al., 2022. Chemical constituents, driving factors, and source apportionment of oxidative potential of ambient fine particulate matter in a Port city in east China. J. Hazard Mater. 440, 129864.

Chow, J.C., Watson, J.G., Lowenthal, D.H., Chen, L.W.A., Zielinska, B., Mazzoleni, L.R., Magliano, K.L., 2007. Evaluation of organic markers for chemical mass balance source apportionment at the Fresno supersite. Atmos. Chem. Phys. 7 (7), 1741–1754.

Corvalan, C., Hales, S., McMichael, A.J., 2005. Ecosystems and Human well-being: Health Synthesis. World health organization.

Costabile, F., Gualtieri, M., Rinaldi, M., Canepari, S., Vecchi, R., Massimi, L., et al., 2023. Exposure to urban nanoparticles at low PM 1 concentrations as a source of oxidative stress and inflammation. Sci. Rep. 13 (1), 18616.

Crippa, M., Canonaco, F., Lanz, V.A., Äijälä, M., Allan, J.D., Carbone, S., et al., 2014. Organic aerosol components derived from 25 AMS data sets across Europe using a consistent ME-2 based source apportionment approach. Atmos. Chem. Phys. 14 (12), 6159–6176.

Crobeddu, B., Aragao-Santiago, L., Bui, L.C., Boland, S., Squiban, A.B., 2017. Oxidative potential of particulate matter 2.5 as predictive indicator of cellular stress. Environ. Pollut. 230, 125–133.

Cusano, M., Gaeta, A., Morelli, R., Cattani, G., Canepari, S., Massimi, L., Leone, G., 2025. Spatial modeling of trace element concentrations in PM10 using generalized additive models (GAMs). Atmosphere 16 (4), 464.

Daellenbach, K.R., Uzu, G., Jiang, J., Cassagnes, L.E., Leni, Z., Vlachou, A., et al., 2020. Sources of particulate-matter air pollution and its oxidative potential in Europe. Nature 587 (7834), 414–419.

Di Iulio, G., Gualtieri, M., Rinaldi, M., Paglione, M., Canepari, S., Massimi, L., Frezzini, M.A., Costabile, F., 2025. Association of PILS-based and filter-based particle-bound reactive oxygen species with urban nanoparticles, secondary organic aerosols, and in-vitro oxidative responses. Environ. Pollut., 126874

Di Martino, E., Massimi, L., Zara, A., Winkler, A., Spagnuolo, L., Ceci, A., et al., 2026. Brake dust from vehicular and rail traffic: assessment of elemental profiles, magnetic susceptibility, dispersion, contributions to soil contamination and health risks. Atmosphere 17 (1), 114.

Dominutti, P.A., Borlaza, L.J.S., Sauvain, J.J., Ngoc Thuy, V.D., Houdier, S., Suarez, G., Jaffrezo, J.L., Tobin, S., Trébuchon, C., Socquet, S., Moussu, E., Mary, G., Uzu, G., 2023. Source apportionment of oxidative potential depends on the choice of the assay: insights into 5 protocols comparison and implications for mitigation measures. Environmental Science: Atmospheres 3 (10), 1497–1512. https://doi.org/10.1039/d3ea00007a.

Expósito, A., Vaccarella, E., Massimi, L., Santibáñez, M., Fernández-Olmo, I., 2025. Size-segregated particulate matter oxidative potential near a ferromanganese plant: associations with soluble and insoluble elements and their sources. Atmos. Pollut. Res. 16 (1), 102330.

Fadel, M., Courcot, D., Delmaire, G., Roussel, G., Afif, C., Ledoux, F., 2023. Source apportionment of PM2. 5 oxidative potential in an East Mediterranean site. Sci. Total Environ. 900, 165843.

Fang, T., Verma, V., Bates, J.T., Abrams, J., Klein, M., Strickland, M.J., et al., 2016. Oxidative potential of ambient water-soluble PM 2.5 in the southeastern United States: contrasts in sources and health associations between ascorbic acid (AA) and dithiothreitol (DTT) assays. Atmos. Chem. Phys. 16 (6), 3865–3879.

Ferrero, L., Cappelletti, D., Moroni, B., Sangiorgi, G., Perrone, M.G., Crocchianti, S., Bolzacchini, E., 2012. Wintertime aerosol dynamics and chemical composition across the mixing layer over basin valleys. Atmos. Environ. 56, 143–153.

Frezzini, M.A., De Francesco, N., Massimi, L., Canepari, S., 2022. Effects of operating conditions on PM oxidative potential assays. Atmos. Environ. 268, 118802.

Grange, S.K., Uzu, G., Weber, S., Jaffrezo, J.L., Hueglin, C., 2022. Linking Switzerland's PM 10 and PM 2.5 oxidative potential (OP) with emission sources. Atmos. Chem. Phys. 22 (10), 7029–7050.

Guerrini, R., 2012. Qualità dell'aria nella provincia di Terni tra il 2002 e il 2011. Quad. ARPA Umbria 33, 81–87.

Happo, M.S., Salonen, R.O., Hälinen, A.I., Jalava, P.I., Pennanen, A.S., Dormans, J.A.M. A., Gerlofs-Nijland, M.E., Cassee, F.R., Kosma, V.-M., Sillanpää, M., Hillamo, R., Hirvonen, M.R., 2010. Inflammation and tissue damage in mouse lung by single and repeated dosing of urban air coarse and fine particles collected from six European cities. Inhal. Toxicol. 22 (5), 402–416.

He, L., Zhang, J., 2023. Particulate matter (PM) oxidative potential: measurement methods and links to PM physicochemical characteristics and health effects. Crit. Rev. Environ. Sci. Technol. 53 (2), 177–197.

Hopke, P.K., Dai, Q., Li, L., Feng, Y., 2020. Global review of recent source apportionments for airborne particulate matter. Sci. Total Environ. 740, 140091. https://doi.org/10.1016/j.scitotenv.2020.140091. Epub 2020 Jun 9. PMID: 32559544; PMCID: PMC7456793.

Huang, W., Zhang, Y., Zhang, Y., Fang, D., Schauer, J.J., 2016. Optimization of the measurement of particle-bound reactive oxygen species with 2′, 7′-dichlorofluorescin (DCFH). Water, Air, Soil Pollut. 227 (5), 164.

In 't Veld, M., Pandolfi, M., Amato, F., Pérez, N., Reche, C., Dominutti, P., Jaffrezo, J., Alastuey, A., Querol, X., Uzu, G., 2023. Discovering oxidative potential (OP) drivers of atmospheric PM10, PM2.5, and PM1 simultaneously in North-Eastern Spain. Sci. Total Environ. 857. https://doi.org/10.1016/j.scitotenv.2022.159386.

Jain, S., Sharma, S.K., Choudhary, N., Masiwal, R., Saxena, M., Sharma, A., et al., 2017. Chemical characteristics and source apportionment of PM 2.5 using PCA/APCS, UNMIX, and PMF at an urban site of Delhi, India. Environ. Sci. Pollut. Control Ser. 24, 14637–14656.

Jeong, J.H., Shon, Z.H., Kang, M., Song, S.K., Kim, Y.K., Park, J., Kim, H., 2017. Comparison of source apportionment of PM2. 5 using receptor models in the main hub port city of East Asia: busan. Atmos. Environ. 148, 115–127.

Kam, W., Delfino, R.J., Schauer, J.J., Sioutas, C., 2013. A comparative assessment of PM 2.5 exposures in light-rail, subway, freeway, and surface street environments in Los Angeles and estimated lung cancer risk. Environ. Sci. Process. Impacts 15 (1), 234–243.

Kaur, M., Chandel, J., Malik, J., Naura, A.S., 2022. Particulate matter in COPD pathogenesis: an overview. Inflamm. Res. 71 (7–8), 797–815.

Kyung, S.Y., Jeong, S.H., 2020. Particulate-matter related respiratory diseases. Tuberc. Respir. Dis. 83 (2), 116.

Lanz, V.A., Alfarra, M.R., Baltensperger, U., Buchmann, B., Hueglin, C., Szidat, S., et al., 2008. Source attribution of submicron organic aerosols during wintertime inversions by advanced factor analysis of aerosol mass spectra. Environ. Sci. Technol. 42 (1), 214–220.

Li, Yuezhao, Chen, Haiyang, Teng, Yanguo, 2020. Source apportionment and source-oriented risk assessment of heavy metals in the sediments of an urban river-lake system. Sci. Total Environ. 737, 140310.

Linares, C., Culqui, D., Belda, F., López-Bueno, J.A., Luna, Y., Sánchez-Martínez, G., et al., 2021. Do Saharan Dust Intrusions Affect the Incidence and Severity of COVID-19 in Spain?.

Linares, C., Díaz, J., Navas, M.A., López-Bueno, J.A., 2025. Does the new European union air quality directive really protect health? A nationwide case study in Spain. Sci. Total Environ. 970, 179002.

Lionetto, M.G., Guascito, M.R., Giordano, M.E., Caricato, R., De Bartolomeo, A.R., Romano, M.P., et al., 2021. Oxidative potential, cytotoxicity, and intracellular oxidative stress generating capacity of PM10: a case study in south of Italy. Atmosphere 12 (4), 464.

Liu, B., Wu, J., Zhang, J., Wang, L., Yang, J., Liang, D., et al., 2017. Characterization and source apportionment of PM2. 5 based on error estimation from EPA PMF 5.0 model at a medium city in China. Environ. Pollut. 222, 10–22.

Marinelli, A., Amato, F., Canepari, S., Massimi, L., di Giosa, A.D., 2026. Contributions to atmospheric particulate matter from different appliances for biomass burning home heating. Atmos. Pollut. Res., 102983

Massimi, L., Frezzini, M.A., Amoroso, A., Di Giosa, A.D., Martino, L., Tiraboschi, C., Messi, M., Astolfi, M.L., Perrino, C., Canepari, S., 2024. Spatially resolved chemical data for PM10 and oxidative potential source apportionment in urban-industrial settings. Urban Clim. 57.

Massimi, L., Perrino, C., Frezzini, M.A., Canepari, S., 2025. Two-year monitoring of indoor/outdoor PM10 at 15 sites in an urban setting. Part II: source apportionment and oxidative potential. Urban Clim. 61, 102466.

Massimi, L., Pietrantonio, E., Astolfi, M.L., Canepari, S., 2022b. Innovative experimental approach for spatial mapping of source-specific risk contributions of potentially toxic trace elements in PM10. Chemosphere 307, 135871.

Massimi, L., Pietrodangelo, A., Frezzini, M.A., Ristorini, M., De Francesco, N., Sargolini, T., et al., 2022a. Effects of COVID-19 lockdown on PM10 composition and sources in the Rome Area (Italy) by elements' chemical fractionation-based source apportionment. Atmos. Res. 266, 105970.

Massimi, L., Ristorini, M., Astolfi, M.L., Perrino, C., Canepari, S., 2020b. High resolution spatial mapping of element concentrations in PM10: a powerful tool for localization of emission sources. Atmos. Res. 244, 105060.

Massimi, L., Ristorini, M., Simonetti, G., Frezzini, M.A., Astolfi, M.L., Canepari, S., 2020a. Spatial mapping and size distribution of oxidative potential of particulate matter released by spatially disaggregated sources. Environ. Pollut. 266.

Massimi, L., Simonetti, G., Buiarelli, F., Di Filippo, P., Pomata, D., Riccardi, C., et al., 2020c. Spatial distribution of levoglucosan and alternative biomass burning tracers in atmospheric aerosols, in an urban and industrial hot-spot of central Italy. Atmos. Res. 239, 104904.

Melzi, G., Massimi, L., Frezzini, M.A., Iulini, M., Tarallo, N., Rinaldi, M., et al., 2024. Redox-activity and in vitro effects of regional atmospheric aerosol pollution: seasonal differences and correlation between oxidative potential and in vitro toxicity of PM1. Toxicol. Appl. Pharmacol. 485, 116913.

Molina, C., Toro A, R., Manzano, C.A., Canepari, S., Massimi, L., Leiva-Guzmán, M.A., 2020. Airborne aerosols and human health: leapfrogging from mass concentration to oxidative potential. Atmosphere 11 (9), 917.

Moroni, B., Ferrero, L., Crocchianti, S., Perrone, M.G., Sangiorgi, G., Bolzacchini, E., Cappelletti, D., 2013. Aerosol dynamics upon Terni basin (Central Italy): results of integrated vertical profile measurements and electron microscopy analyses. Rendiconti Lincei 24 (4), 319–328.

Namgung, H.G., Kim, J.B., Woo, S.H., Park, S., Kim, M., Kim, M.S., et al., 2016. Generation of nanoparticles from friction between railway brake disks and pads. Environ. Sci. Technol. 50 (7), 3453–3461.

Ngoc Thuy, V.D., Jaffrezo, J.-L., Hough, I., Dominutti, P.A., Salque Moreton, G., Gille, G., Francony, F., Patron-Anquez, A., Favez, O., Uzu, G., 2024. Unveiling the optimal regression model for source apportionment of the oxidative potential of PM 10. Atmos. Chem. Phys. 24 (12), 7261–7282.

Norris, Gary, Duvall, Rachelle, Brown, Steve, Bai, Song, 2014. EPA Positive Matrix Factorization (PMF) 5.0 Fundamentals and User Guide. US Environmental Protection Agency, Washington, DC. EPA/600/R-14/108.

Novák, J., Vaculovič, A., Klánová, J., Giesy, J.P., Hilscherová, K., 2020. Seasonal variation of endocrine disrupting potentials of pollutant mixtures associated with various size-fractions of inhalable air particulate matter. Environ. Pollut. 264, 114654.

Owoade, K.O., Hopke, P.K., Olise, F.S., Ogundele, L.T., Fawole, O.G., Olaniyi, B.H., et al., 2015. Chemical compositions and source identification of particulate matter (PM2. 5 and PM2. 5–10) from a scrap iron and steel smelting industry along the Ife–Ibadan highway, Nigeria. Atmos. Pollut. Res. 6 (1), 107–119.

Paatero, P., 1999. The multilinear engine—a table-driven, least squares program for solving multilinear problems, including the n-way parallel factor analysis model. J. Comput. Graph Stat. 8 (4), 854–888.

Paatero, P., Hopke, P.K., 2003. Discarding or downweighting high-noise variables in factor analytic models. Anal. Chim. Acta 490 (1–2), 277–289.

Pant, P., Harrison, R.M., 2013. Estimation of the contribution of road traffic emissions to particulate matter concentrations from field measurements: a review. Atmos. Environ. 77, 78–97.

Perez, L., Tobias, A., Querol, X., Künzli, N., Pey, J., Alastuey, A., et al., 2008. Coarse particles from Saharan dust and daily mortality. Epidemiology 19 (6), 800–807.

Pernigotti, D., Belis, C.A., Spanò, L., 2016. SPECIEUROPE: the European data base for PM source profiles. Atmos. Pollut. Res. 7 (2), 307–314.

Perrino, C., Catrambone, M., Canepari, S., 2020. Chemical composition of PM10 in 16 urban, industrial and background sites in Italy. Atmosphere 11 (5), 479.

Perrino, C., Massimi, L., Giusto, M., Sargolini, T., Ristorini, M., Canepari, S., 2025. Two-year monitoring of indoor and outdoor PM10 at 15 sites in an urban setting. Part I: chemical composition and source tracers. Urban Clim. 61, 102464.

Pietrogrande, M.C., Romanato, L., Russo, M., 2022. Synergistic and antagonistic effects of aerosol components on its oxidative potential as predictor of particle toxicity. Toxics 10 (4). https://doi.org/10.3390/toxics10040196.

Plunk, E.C., Richards, S.M., 2020. Endocrine-disrupting air pollutants and their effects on the hypothalamus-pituitary-gonadal axis. Int. J. Mol. Sci. 21 (23), 9191.

Polissar, A.V., Hopke, P.K., Paatero, P., Malm, W.C., Sisler, J.F., 1998. Atmospheric aerosol over Alaska: 2. Elemental composition and sources. J. Geophys. Res. Atmos. 103 (D15), 19045–19057.

Pétremand, R., Suárez, G., Besançon, S., Dil, J.H., Guseva Canu, I., 2022. A real-time comparison of four particulate matter size fractions in the personal breathing zone of Paris subway workers: a six-week prospective study. Sustainability 14 (10), 5999.

Querol, X., Moreno, T., Karanasiou, A., Reche, C., Alastuey, A., Viana, M., et al., 2012. Variability of levels and composition of PM 10 and PM 2.5 in the Barcelona metro system. Atmos. Chem. Phys. 12 (11), 5055–5076.

Rychlik, K.A., Secrest, J.R., Lau, C., Pulczinski, J., Zamora, M.L., Leal, J., et al., 2019. In utero ultrafine particulate matter exposure causes offspring pulmonary immunosuppression. Proc. Natl. Acad. Sci. 116 (9), 3443–3448.

Sanda, M., Dunea, D., Iordache, S., Predescu, L., Predescu, M., Pohoata, A., Onutu, I., 2023. Recent urban issues related to particulate matter in Ploiesti City, Romania. Atmosphere 14 (4), 746.
Santibáñez-Andrade, M., Quezada-Maldonado, E.M., Rivera-Pineda, A., Chirino, Y.I., García-Cuellar, C.M., Sánchez-Pérez, Y., 2023. The road to malignant cell transformation after particulate matter exposure: from oxidative stress to genotoxicity. Int. J. Mol. Sci. 24 (2), 1782.
Schraufnagel, D.E., Balmes, J.R., Cowl, C.T., De Matteis, S., Jung, S.H., Mortimer, K., et al., 2019a. Air pollution and noncommunicable diseases: a review by the Forum of International respiratory societies' environmental committee, Part 2: air pollution and organ systems. Chest 155 (2), 417–426.
Schraufnagel, D.E., Balmes, J.R., Cowl, C.T., De Matteis, S., Jung, S.H., Mortimer, K., et al., 2019b. Air pollution and noncommunicable diseases: a review by the forum of international respiratory societies' Environmental Committee, part 1: the damaging effects of air pollution. Chest 155 (2), 409–416.
Seinfeld, J.H., Pandis, S.N., 2006. Atmospheric Chemistry and Physics: from Air Pollution to Climate Change, second ed. John Wiley & Sons, New York.
SENTIERI - studio Epidemiologico Nazionale dei Territori e degli Insediamenti Esposti a Rischio da Inquinamento: l'incidenza del mesotelioma, Epidemiologia&Prevenzione, 2016.
SENTIERI - studio epidemiologico nazionale dei territori e degli insediamenti esposti a rischio da inquinamento, Quinto Rapporto. Epidemiologia&Prevenzione, 2019.
SENTIERI - studio epidemiologico nazionale dei territori e degli insediamenti esposti a rischio da inquinamento, Sesto Rapporto. Epidemiologia&Prevenzione, 2023.
Serafeim, E., Besis, A., Kouras, A., Farias, C.N., Yera, A.B., Pereira, G.M., Samara, C., de Castro Vasconcellos, P., 2023. Oxidative potential of ambient PM2.5 from São Paulo, Brazil: variations, associations with chemical components and source apportionment. Atmos. Environ. 298.
Shen, J., Taghvaee, S., La, C., Oroumiyeh, F., Liu, J., Jerrett, M., et al., 2022. Aerosol oxidative potential in the greater Los Angeles area: source apportionment and associations with socioeconomic position. Environ. Sci. Technol. 56 (24), 17795–17804.
Simoneit, B.R., Elias, V.O., Kobayashi, M., Kawamura, K., Rushdi, A.I., Medeiros, P.M., et al., 2004. Sugars dominant water-soluble organic compounds in soils and characterization as tracers in atmospheric particulate matter. Environ. Sci. Technol. 38 (22), 5939–5949.
Simonetti, G., Conte, E., Perrino, C., Canepari, S., 2018. Oxidative potential of size-segregated PM in an urban and an industrial area of Italy. Atmos. Environ. 187, 292–300.
Simpson, I.J., Meinardi, S., Blake, D.R., Blake, N.J., Rowland, F.S., Atlas, E., Flocke, F., 2002. A biomass burning source of C1–C4 alkyl nitrates. Geophys. Res. Lett. 29 (24).
Soleimanian, E., Taghvaee, S., Mousavi, A., Sowlat, M.H., Hassanvand, M.S., Yunesian, M., et al., 2019. Sources and temporal variations of coarse particulate matter (PM) in Central Tehran, Iran. Atmosphere 10 (5), 291.
Song, W., Liu, X.Y., 2023. Source oxygen contributions of primary nitrate emitted from biomass burning. Sci. Total Environ. 854, 158736.
Sullivan, A.P., Holden, A.S., Patterson, L.A., McMeeking, G.R., Kreidenweis, S.M., Malm, W.C., et al., 2008. A method for smoke marker measurements and its potential application for determining the contribution of biomass burning from wildfires and prescribed fires to ambient PM2. 5 organic carbon. J. Geophys. Res. Atmos. 113 (D22).
Szigeti, T., Óvári, M., Dunster, C., Kelly, F.J., Lucarelli, F., Záray, G., 2015. Changes in chemical composition and oxidative potential of urban PM2. 5 between 2010 and 2013 in Hungary. Sci. Total Environ. 518, 534–544.
Taiwo, A.M., Harrison, R.M., Shi, Z., 2014. A review of receptor modelling of industrially emitted particulate matter. Atmos. Environ. 97, 109–120.
Tositti, L., Moroni, B., Dinelli, E., Morozzi, P., Brattich, E., Sebastiani, B., et al., 2020. Deposition processes over complex topographies: experimental data meets atmospheric modeling. Sci. Total Environ. 744, 140974.
Union, P., 2008. Directive 2008/50/EC of the European Parliament and of the Council of 21 May 2008 on Ambient Air Quality and Cleaner Air for Europe. Official Journal of the European Union.
Vaccarella, E., Lucchesi, V., Canepari, S., Massimi, L., Bellini, R., Porretta, D., Mastrantonio, V., 2025b. An in vivo assessment revealed multiple toxic effects of brake dust on the urban mosquito Aedes albopictus. Sci. Total Environ. 991, 179937.
Vaccarella, E., Massimi, L., Canepari, S., 2025. Assessment of oxidative stress induced by atmospheric particulate matter: from acellular and cellular assays to the use of model and experimental organisms. Sci. Total Environ. 965, 178651.
Verma, V., Fang, T., Xu, L., Peltier, R.E., Russell, A.G., Ng, N.L., Weber, R.J., 2015. Organic aerosols associated with the generation of reactive oxygen species (ROS) by water-soluble PM2. 5. Environ. Sci. Technol. 49 (7), 4646–4656.
Vernocchi, V., Brunoldi, M., Canepari, S., Corsini, E., Isolabella, T., Massimi, L., et al., 2025. Oxidative potential and cellular toxicity of carbonaceous aerosols undergoing aging in an atmospheric simulation chamber. Toxicol. Appl. Pharmacol., 117573
Vimukthi, W.P.D., Dong, S., Yang, C., Zhang, Y., Baikeri, G., Lou, T., Cao, F., 2025. Enhancing DTT assays for reactive oxygen species detection in atmospheric particulate matter: key factors and methodological insights. Environmental Science: Atmospheres 5 (8), 865–878.
Øvrevik, J., 2019. Oxidative potential versus biological effects: a review on the relevance of cell-free/abiotic assays as predictors of toxicity from airborne particulate matter. Int. J. Mol. Sci. 20 (19), 4772.
Weber, S., Uzu, G., Calas, A., Chevrier, F., Besombes, J.L., Charron, A., et al., 2018. An apportionment method for the oxidative potential of atmospheric particulate matter sources: application to a one-year study in Chamonix, France. Atmos. Chem. Phys. 18 (13), 9617–9629.
Weber, S., Uzu, G., Favez, O., Borlaza, L.J.S., Calas, A., Salameh, D., et al., 2021. Source apportionment of atmospheric PM 10 oxidative potential: synthesis of 15 year-round urban datasets in France. Atmos. Chem. Phys. 21 (14), 11353–11378.
World Health Organization, 2021. WHO Global Air Quality Guidelines: Particulate Matter (PM2. 5 and PM10), Ozone, Nitrogen Dioxide, Sulfur Dioxide and Carbon Monoxide: Executive Summary.
Xu, Bo, Xu, Han, Zhao, Huan, Gao, Jie, Liang, Danni, Yue, Li, Wang, Wei, Feng, Yinchang, Shi, Guoliang, 2023. Source apportionment of fine particulate matter at a megacity in China, using an improved regularization supervised PMF model. Sci. Total Environ. 879, 163198.
Xu, J., Liu, D., Wu, X., Vu, T.V., Zhang, Y., Fu, P., et al., 2021. Source apportionment of fine organic carbon at an urban site of Beijing using a chemical mass balance model. Atmos. Chem. Phys. 21 (9), 7321–7341.
Zhao, Qiuyue, Bi, Jun, Liu, Qian, Ling, Zhenghao, Shen, Guofeng, Chen, Feng, Qiao, Yuezhen, Li, Chunyan, Ma, Zongwei, 2020. Sources of volatile organic compounds and policy implications for regional ozone pollution control in an urban location of Nanjing, East China. Atmos. Chem. Phys. 20 (6), 3905–3919.